AD

DEFECT CHARACTERISATION OF ULTRA-SMALL DEVICES

Final Technical Report
by

David J. Keeble

(9/99)

United States Army

EUROPEAN RESEARCH OFFICE OF THE U.S. ARMY

London, England

CONTRACT NUMBER N68171-97-M-5770

R+D no: 8224-EE-01.

David J. Keeble

Approved for Public Release; distribution unlimited

20000118 070

	Form Approved
REPORT DOCUMENTATION PAGE	OMB No. 0704-0188

Public reporting burden for this collection of information is estimated to average 1 hour per response, including the time for reviewing instructions, searching existing data sources gathering and maintaining the data needed, and completing and reviewing the collection of information. Send comments regarding this burden estimate or any other aspect of this collection of information, including suggestions for reducing this burden, to Washington Headquarters Services, Directorate for information Operations and Reports, 1215 Jefferson Davis Highway, Suite 1204 Arlington, VA 22202-4302, and to the Office of Management and Budget, Paperwork Reduction Project (0704-0188), Washington, DC 20503.

1. AGENCY USE ONLY (Leave Blank)	2. REPORT DATE 20th September 1999	3. REPORT TYPE AND DATES COVERED Final, September 1997 – November 1998

4. TITLE AND SUBTITLE Defect characterization of ultra-small devices	5. FUNDING NUMBERS N68171-97-M-5770, 8224-EE-018

6. AUTHOR(S)

D J KEEBLE

7. PERFORMING ORGANIZATION NAME(S) AND ADDRESS(ES) University of Dundee, Department of Applied Physics and Electronic & Mechanical Engineering, Dundee, DD1 4HN, Scotland.	8. PERFORMING ORGANIZATION REPORT NUMBER ERO-1F

9. SPONSORING/MONITORING AGENCY NAME(S) AND ADDRESS(ES) US Army European Research Office, 223 Old Marylebone Road, London, NW1 5TH	10. SPONSORING /MONITORING AGENCY REPORT NUMBER

11. SUPPLEMENTARY NOTES

12a. DISTRIBUTION/AVAILABILITY STATEMENT	12b. DISTRIBUTION CODE

13. ABSTRACT (Maximum 200 words)

The work described here details the development of electron magnetic resonance facilities and measurements for use on US Army projects for the characterisation of electronic devices. An operational electrically-detected magnetic resonance (EDMR) spectrometer constructed has been installed based on a Bruker (B_{max} = 2.1 T) electromagnet. The first spectra from device structures have been successfully recorded. A flexible modular spectrometer system has resulted and has led to further work to develop the instrumentation. Initial measurements on commercial silicon n^+p diodes are consistent with previous studies. Evidence that the origin of the EDMR signal is due to platinum is assessed with the aid of spectral simulation. Electron paramagnetic resonance spectra were simulated by exact diagonalisation of the appropriate spin-Hamiltonians. No completely satisfactory correspondence between reported EPR spectra and the measured and reported EDMR spectra was found. The long-term aim of the work is to study localisation in quantum confined structures and to investigate electrically detected magnetic resonance for impurity and defect detection in operational device structures. Further, the possibility that the technique will give key insights into spin processes in semiconductors of direct relevance to the implementation of quantum computing devices will also be explored.

14. SUBJECT ITEMS Electrically Detected Magnetic Resonance, EDMR		15. NUMBER OF PAGES
		16. PRICE CODE

17. SECURITY CLASSIFICATION OF REPORT Unclassified	18. SECURITY CLASSIFICATION OF THIS PAGE Unclassified	19. SECURITY CLASSIFICATION OF ABSTRACT Unclassified	20. LIMITATION OF ABSTRACT

NSN 7540-01-280-5500

Standard Form 298 (Rev. 2-89)
Prescribed by ANSI Std. Z39-18
298-102

ATTACHMENT 1 PAGE 1

SUMMARY

The work described here details the development of electron magnetic resonance facilities and measurements for use on U.S. Army projects for the characterisation of electronic devices. An operational electrically-detected magnetic resonance (EDMR) spectrometer constructed has been installed based on a Bruker (B_{max} = 2.1 T) electromagnet. The first spectra from device structures have been successfully recorded. A flexible modular spectrometer system has resulted and has led to further work to develop the instrumentation. Initial measurements on commercial silicon n^+p diodes are consistent with previous studies. Evidence that the origin of the EDMR signal is due to platinum is assessed with the aid of spectral simulation. Electron paramagnetic resonance spectra were simulated by exact diagonalisation of the appropriate spin-Hamiltonians. No completely satisfactory correspondence between reported EPR spectra and the measured and reported EDMR spectra was found. The long-term aim of the work is to study localisation in quantum confined structures and to investigate electrically detected magnetic resonance for impurity and defect detection in operational device structures. Further, the possibility that the technique will give key insights into spin processes in semiconductors of direct relevance to the implementation of quantum computing devices will also be explored.

Table of Contents

Introduction

The major drive in electronics technology is the production of ever smaller feature sizes. In consequence the necessity to control impurity and native defect concentrations is increasing. While the presence of such defects may be inferred from the degradation of device characteristics, especially for devices with very reduced dimension, their chemical nature can not be determined. Chemical identification requires spectroscopic information that can not be supplied by conventional defect sensitive electrical methods (e.g. Deep Level Transient Spectroscopy (DLTS) and related techniques). There is a need for a defect-sensitive technique that gives spectroscopic information capable of chemical identification of the defect site but which can be performed on an operational device. Further, such a technique should have the potential for application to devices with dimensions down to the nanometer scale.

Electrically detected magnetic resonance (EDMR) has demonstrated that it can detect defects in operational devices and give spectroscopic information. [1,2] The spectra contain information similar to those from electron paramagnetic resonance (EPR) in that they exhibit anisotropy characteristic of the centre's symmetry, and show hyperfine and superhyperfine splittings due to interactions with surrounding magnetic nuclei. The importance of metal ion contamination in semiconductor device production has re-emerged as an area of importance. EDMR has been shown to be sensitive to metal ions. [1,3,4]

The limit on the number of detectable centres imposed by statistical physics on EPR of order 10^{11} defects does not apply, since detection is not direct detection of absorbed photons but results from spin-dependent recombination processes. Recent experiments on thin-film transistors have shown the technique to be capable of detecting as few as 10^6 defects. [5,6] These experiments support the proposal made by the author that the technique should, in principle, be capable of defect detection in small-scale device structures. [7]

Recent developments in quantum computing also relate to this work. The desire to have devices implemented using semiconductor technology have progressed recently with the preparation and transport of specific spin states in and through semiconductor structures. Solid state implementation of quantum computing requires devices capable of spin control of carrier transport to allow efficient integration into necessary circuitry. EDMR is sensitive both to spin dependent recombination and spin dependent transport/scattering processes so holds the prospect of giving new insights relevant to quantum computing.

This report describes the initial phase of a programme to install a multifrequency purpose built electrically detected magnetic resonance facility. In addition the issues are raised regarding the interpretation of spectral information from EDMR. While, as outlined above, the technique provides similar spectral information to Electron Paramagnetic Resonance (EPR) the direct correspondence between the spectral information supplied by the two techniques has not been clearly established. This can be related to the lack, despite significant advances, of a fully consistent theory for the EDMR mechanism. [8] This report also includes a detailed review of EPR studies of platinum in silicon with spectral simulations reproducing expected behaviour on rotation of the applied magnetic field within the (111) plane. In performing EDMR experiments on commercial diode structures it is this plane that can most readily be studied.

Introduction to EDMR

This section outlines the development models for the EDMR mechanism up to, and including, that of Rong *et al.* [8] It is not, however, a comprehensive review of the EDMR literature, the aim is to give non-experts a background to the central concepts.

The first observation of spin dependent transport effects in semiconductors was by Honig [9]. Hoing recognised that carrier transport in a semiconductor doped with, for instance hydrogenic-type, neutral impurities would be expected to be dependent on the polarisation of the carriers and the electrons of the neutral impurities. The scattering cross section for an electron scattering from neutral hydrogen contains both singlet and triplet contributions, conductivity is then a function of polarisation. Carrier polarisation, P, resulting from Boltzmann equilibrium is given by $P = \tanh(g\beta B/kT)$ where g is the gyromagnetic ratio, β the Bohr magnetron and B the applied magnetic field. For a moderate applied field, B = 1.2 T, at low temperature, T = 0.4 K, with $g \approx 2$ high values of polarisation can be obtained, P = 0.97, insuring almost complete triplet scattering. If carrier spin-lattice relaxation times are long then the polarisation dependence of the conductivity can be studied by transient switching of the applied magnetic field from which the relaxation time can be measured and information on scattering lengths obtained.

Hoing also proposed that, with the application of monochomatic microwaves, electron paramagnetic resonance could be detected. If the microwave power level is such to induce saturation at resonance, increasing the spin temperature, then on sweeping the magnetic field through a paramagnetic transition of the neutral impurity the polarisation is reduced due to the 'spin mixing'. Maxwell and Hoing performed the first Electrical Detected Magnetic Resonance (EDMR) experiment on lightly phosphorus doped float-zone silicon and were able to detect the phosphorous hyperfine doublet by studying variations in the low temperature photocurrent. [10]

Lepine realised that similar arguments could apply to carrier recombination in semiconductors, and were valid when this process involved a recombination centre. The spin dependent recombination through the paramagnetic state of a localised recombination centre, detected by a resonant change in the photocurrent in silicon was reported. [11] A more detailed study showed the recombination centres detected were surface states. [12] A simple model to explain the spin dependence of the recombination was outlined and is similar to that outlined by Hoing but for the simpler situation of carrier capture rather than scattering. The description of the model outlined below follows Solomon. [13]

Because of conservation of angular momentum in an electron-hole collision, it is expected that the recombination will be dependent on the spin-state of the carriers. This is illustrated for the hypothetical case of direct electron hole recombination in Figure 1. For low energy carriers the collision is mostly S-like (L = 0) and the recombination of the triplet state is forbidden since the total spin, $S_{total} = 1$, cannot disappear in the electron-hole annihilation when clearly $S_{total} = 0$. This argument is unchanged when the more realistic case of a recombination centre is considered. In the Shockley-Read model an electron, for example, is first trapped on a deep centre. The trapped electron then captures a free hole, completing the recombination. Here, also,

7

the trapped electron can only recombine with a hole of opposite spin ($S_{total} = 0$) to conserve total angular momentum after recombination.

In consequence than it is expected that the triplet recombination rate, W_T, will be zero, or at least much smaller than the singlet recombination, W_S. In zero field, the spin directions of the injected carriers are random (spin polarizations zero) and the probabilities of a singlet or triplet electron-hole spin state are respectively ¼ and ¾, as follows for the distribution of states for a system of two spin-1/2 particles. The recombination rate is then

$$W_{random} = \frac{1}{4}W_S + \frac{3}{4}W_T$$

where clearly $W_T \ll W_S$. If the spins of the carriers have polarizations P_e and P_h as will be the case, for example, in an applied magnetic field, the probabilities of singlet or triplet electron-hole spin statistics depart slightly from the values ¼ and ¾. They are given, for spin ½, by the average values of the projection operators

$$\pi_S = \frac{1}{4} - \mathbf{S}_e \cdot \mathbf{S}_h$$
$$\pi_T = \frac{3}{4} + \mathbf{S}_e \cdot \mathbf{S}_h$$

where $\mathbf{S}_e$ and $\mathbf{S}_h$ are the spins of the recombining electron and hole. For uncorrelated spins, the average values are simply given by

$$\langle \mathbf{S}_e \rangle = \mathbf{P}_e / 2, \quad \langle \mathbf{S}_h \rangle = \mathbf{P}_h / 2$$

so that the recombination rate is now

$$W = \frac{W_S}{4}\left(1 - \mathbf{P}_e \cdot \mathbf{P}_h\right) + \frac{W_T}{4}\left(3 + \mathbf{P}_e \cdot \mathbf{P}_h\right) + W',$$

where a hypothetical spin-independent process W' had been added for the sake of generality. The recombination rate can also be expressed as

$$W = W_0\left(1 - \alpha \mathbf{P}_e \cdot \mathbf{P}_h\right),$$

with $W_0 = (W_S + 3W_T + 4W')/4$, and $\alpha = \dfrac{W_S + W_T}{W_S + 3W_T + 4W'}$.

In this model it should be noted that $\alpha \leq 1$, with the maximum value $\alpha = 1$ being obtained when the "leakage" processes W_T and W' are zero.

A change of the spin polarisation of the electron (or hole) will result in a change of the recombination rate that can be detected, for example, by a small variation of photoconductivity. This is usually accomplished by "saturation" of the electron paramagnetic resonance. [14] In the

absence of a microwave field, the polarisation relaxes towards its equilibrium value $P_0 = \hbar\omega/2kT$ at a rate $1/T_1$ (T_1 is the longitudinal relaxation time and $\hbar\omega$ the spin splitting in the applied magnetic field). At resonance, the microwave field induces transitions at a rate W_{RF}, thus tending to equalise the populations of the spin states and to reduce the spin polarisation. The two competing effects result in a steady-state polarisation

$$P = P_0 \frac{1}{1 + W_{RF}T_1}$$

The quantity W_{RF} is proportional to the microwave power, so, by extrapolation to infinite power, one has effectively a way of "nulling" the polarisation of the resonant spins, the other experimental parameters remaining unchanged. As pointed out by Solomon, based on this simple model provided the recombination is dominated by the spin-dependent process and that the resonance line can be saturated with the available power, the EDMR signal is independent of the number of spins. [13]

However, Lepine [12] had already showed that the magnitude of the effect measured was approximately one order greater that predicted by this simple model and later work confirmed the order of the effect could be in the range 10^{-4}. The maximum variation in recombination rate, assuming complete saturation, is given by

$$\frac{\Delta W}{W} \leq P_e \cdot P_h$$

which for a room temperature experiment performed at 9.5 GHz taking $g \approx 2$ ($B \approx 0.33$ T) predicts $\Delta W/W \approx 10^{-6}$.

The observation of spin dependent photoconductivity in silicon by Lepine stimulated a number of related studies. [11,12] The spin-dependent recombination at surfaces [15] and dislocations [16,17], space charge region of a junction [18], amorphous materials [19] with a few theoretical models to explain the magnitude of the effect [20,21].

White and Gouyet considered the possibility of the formation of a bound electron-hole pair triplet exciton which if initially in the $m_s = -1$ state, and so forbidden to decay to the singlet state necessary for recombination, could be excited to the $m_s = 0$ state by magnetic resonance. [21] They point out such a process is well known in phosphorescent materials where the radiative triplet-to-singlet transition is enhanced by EPR. However, the observation that the decay of the EDMR using photocurrent decays much faster than the EPR signal for amorphous silicon meant such a triplet could not be involved. Instead they proposed a model in which the photogenerated carriers are initially trapped into shallow centres close to the band edges, caused by a local rearrangement, from which they can then trap to deeper states with the emission of N phonons. The microwave resonance acts to heat up the local environment so enhancing phonon emission and trapping to a deep state. The analysis, based in part on multi-phonon trapping, resulted in an approximate expression for the change in recombination rate of

$$\frac{\Delta W}{W} \approx \frac{\tau}{T_1} \frac{\Delta E}{\hbar\omega_0} \frac{1}{N_0} \left(\frac{\beta B}{kT}\right)^2$$

where τ was approximated to be the recombination time, T_1 the spin-lattice relaxation time, ΔE the energy of the deep state from the appropriate band edge, $\hbar\omega_0$ the phonon energy and N_0 the number of atoms making up the local environment of the trap. Using Lepine's [12] value for τ / T_1 of 35 and $\Delta E/\hbar\omega_0 \sim 20$ an enhancement factor of 120 was obtained. The EDMR in the model is assumed to be that of a shallow localised electron. As such it is more extended and therefore interacts more with other localised spins decreasing T_1 relative to that of the deeply trapped more-localised electron.

A significant advance in developing a theoretical understanding of EDMR was made by Kaplan, Solomon and Mott (KSM). [22] As seen above in Lepine's simple model an isotropic distribution of spins results in probabilities of singlet and triplet configurations of ¼ and ¾, respectively. The external magnetic field results in polarisation of the two spin systems and so introduces a degree of anisotropy that can be nulled in an EDMR experiment with a resonant saturating microwave field. Kaplan, Solomon and Mott introduce an alternative source of anisotropy resulting from the formation of an intermediate pair state prior to recombination. This intermediate state requires the carrier pair to be in proximity. The pair can either recombine or dissociate but can not recombine with other carriers. In highly disordered systems such as amorphous semiconductors the concept of a trapped electron with a near neighbour trapped hole is likely valid.

The existence of a carrier pair prior to recombination allows for a spin correlation between the partners, even if the total spin population is still random. In an extreme case where no spin relaxation occurs in the pair-state then pairs created in singlet configurations will have a shorter lifetime and there will be a net surplus of triplet configurations. Resonant absorption by either the electron or hole spin population will return it to an isotropic distribution, so enhancing the recombination rate.

To make an explicit calculation all spin configurations between the singlet and triplet extremes must be considered. Using the conventional vector representation of each spin quantum state a quantum average can be obtained

$$\langle S_e \cdot S_h \rangle = \frac{\cos\theta}{4}$$

where θ is the angle between electron and hole spin vectors. For such a pair the recombination probability per unit time can be written as $W_R(\theta) = W_S \langle \pi_S(\theta) \rangle$ where W_S is the recombination rate for a pair in a pure singlet configuration and the triplet rate is assumed to be zero. The recombination rate then has the form

$$W_R(\theta) = W_S \frac{1 - \cos\theta}{4}.$$

If pairs are created with configurations in the range θ to $\theta + d\theta$ at a rate $c(\theta)$ and dissociate at a rate W_D, assumed to be independent of θ, then the steady state density of pairs with angle θ is given by detailed balance:

$$N(\theta) = \frac{c(\theta)}{W_R(\theta) + W_D}$$

In general $c(\theta)$, appearing in the usual rate equation [23], will depend on the hole concentration p, electron concentration n and possibly on pair concentration $N(\theta)$. To progress further it is required to make some estimate of the creation rate $c(\theta)$. A simple calculation can be made if it is assumed that the possible pairs sites are weakly populated allowing $c(\theta)$ to be independent of the steady state concentration of the pair density $N(\theta)$. Since it has been assumed that the distribution of carrier spins is isotropic then it is reasonable to assume an isotropic distribution for the pair creation rate, which then takes the form

$$c(\theta) = \frac{C}{2}\sin\theta$$

where C is the total creation rate depending only on the concentrations n, p of excess/injected carriers.

It is now possible to estimate the density of pairs as a function of relative spin orientation, $N(\theta)$.

$$N(\theta) = \frac{2C\sin\theta}{4W_D + W_S(1 - \cos\theta)}$$

This can then be compared to the density of pairs expected with the spin interaction between the two carriers 'turned off' so the recombination rate reduces to $W_S/4$. This pair density for random spin orientation is given by

$$N_{RAND}(\theta) = \frac{2C\sin\theta}{4W_D + W_S}$$

The deviation of the pair density for spin correlated pairs against random pairs is can be plotted for different ratios of the singlet recombination rate to the pair dissociation rate, $\lambda = W_D/W_S$.

$$\frac{N(\theta)}{N_{RAND}(\theta)} = \frac{1+4\lambda}{1+4\lambda-\cos\theta}$$

The behaviour is as expected, if the dissociation rate is not too fast the distribution is peaked in the region of $\theta = 0$ showing an excess of triplet configurations. It is now possible to calculate the magnitude of the spin-dependent effect on recombination. The total recombination rate is obtained by summing $N(\theta)W_R(\theta)$ over all θ.

$$R = \int_0^\pi N(\theta)W_R(\theta)d\theta$$

This gives the recombination rate, in terms of $\lambda = W_D/W_S$, as

$$R = C\left[1 - 2\lambda\log\frac{1+2\lambda}{2\lambda}\right].$$

The resonant saturation of either the electron or the hole spin, extrapolated to infinite power, restores the spin-pair random distribution and the pairs recombine at a rate given by the average of $W_R(\theta)$. If the g-values of the electrons and holes are different, the resonant transitions do not conserve the total spin of a pair, thus destroying the correlation between the spin pairs. If the g-values are the same, the random distribution of spin states is obtained through resonant heating of the spin system by the microwave field.

$$W_R(\theta) = W_S\frac{1-\cos\theta}{4}$$

$$\overline{W}_R = \langle W_R(\theta)\rangle = W_S/4$$

The recombination rate at resonant saturation then becomes

$$R_{SAT} = \frac{C}{1+4\lambda}$$

and the relative change in the recombination rate is then

$$\frac{\Delta R}{R} = \frac{R-R_{SAT}}{R}.$$

This can be plotted as a function of $\lambda = W_D/W_S$ and shows a maximum relative change of order 10^{-1} for $\lambda = 0.3$.

The actual magnitude of the effect is expected to be less as the analysis does not take account of the finite triplet recombination rate, the distribution of λ values, the spin-relaxation processes in the pair state, incomplete resonance and the competing recombination mechanisms that do not involve pairs. It was also realised that the exchange interaction between an electron and a hole pair had not been treated. If it is large compared to the difference of their Zeeman energies, the RF field will not change the angle θ. This implies the overlap between the two wavefunctions must be small, but still large enough to allow a finite recombination probability. It contended that for carriers trapped in localised states of sufficient depth, pairs having these properties can certainly exist.

The situation is different if one or both of the carriers are in shallow states. In this case the Coulomb interaction may play a role, and bound pair (exciton) can exist with large overlap. If this is the case and the mean free path is small, the classical analysis of Onsager can be applied where thermal energy can separate the carriers from time to time up to a distance $e^2/\varepsilon_R kT$ without dissociation. At this distance the exchange interaction may be weak enough to allow the RF field to change θ so altering the recombination.

One direct conclusion from the KSM theory is that the magnitude of the EDMR should be independent of resonant frequency, this was indeed found to be the case for EDMR detected using photo-conductivity from silicon through the frequency range 1.9-9.3 GHz.[22] The simple Lepine model, based on thermal equilibrium spin polarisation, predicts that the EDMR signal should increase in magnitude with the square of the magnetic field [$P_e P_h \approx \left(g\beta B/kT\right)^2$], in stark contrast to the observed field independence. This magnetic field independence together with the order of magnitude of the effect clearly indicates the spin polarisation of the recombining electron hole pair is not in thermal equilibrium.

The evident success of the KSM theory justifies a summary of the major points. The theory requires electrons and holes to form localised pairs, wavefunction overlap must be possible. The pairs are created with random spin orientations and those with spin singlet pairs recombine before spin relaxation occurs. The allowed pair recombination rate is much faster than the spin lattice relaxation rate. If the system does not reach thermal equilibrium then there will be an excess of triplet pairs. Application of a resonant microwave field now has the effect of converting some triplet pairs to singlets so enhancing recombination. The important differences in comparison with Lepine's model are the time scales of the spin pair and of the relaxation, this results in a non-thermalised population. These conditions are independent of the magnitude of the applied magnetic field required for spin resonance.

Rong *et al* re-examined KSM theory and discuss some shortcomings of the original formulation. [8] The central feature of a localised electron-hole pair was questioned, localising, shallow trapping, of both the hole and the electron in proximity prior to recombination is plausible in amorphous semiconductors but is questionable in crystalline materials. Spatially correlated deep traps are unlikely unless they form a close donor-acceptor pair type defect. However, in this case recombination is usually very efficient and the exchange interaction between the spins large, so large in fact as to preclude a spin resonant transition connecting singlet to triplet states. In addition evidence existed that recombination through paramagnetic trapping centres in semiconductors detectable by EDMR was consistent with the simple Shockley-Read (SR) model. Carrier capture from one of the bands by a deep trap is followed by capture of a carrier from the other band so the defect centre mediates the recombination. Rong et al outlined how such a process could be consistent with a KSM mechanism.

In a SR mechanism electron or/and hole capture at the deep centre could be spin dependent. The SR model assumes that the limitation in the recombination rate is the availability of electrons and holes entering the traps. However, another limiting factor was admitted, that of the so-called readjustment time of the electron (or hole), the time taken for recombination. The approximation was made that this time is zero, however, for EDMR clearly this can not be the

case. It was proposed that capture first occurs at an excited state of the deep trap, with energy close to the appropriate band-edge. The carrier is now able either to dissociate or to form a weakly-exchange-coupled pair with a carrier trapped at the deep centre. It as assumed the relaxation time of the captured carrier is now much longer than that of a carrier in one of the bands. No spin-lattice relaxation is assumed during the pairing time. The pairing time is the inverse of the dissociation rate, P_d.

In general, the spin-Hamiltonian of such a pair is given by

$$H = H_e + H_h + H_{exchange}$$

where H_e is the spin-Hamiltonian of the excited-state electron, H_h that for the deep hole and $H_{exchange}$ is the exchange interaction between them. A specific example assuming only Zeeman and exchange interactions is given below.

$$H = g_e \mu \mathbf{B} \cdot \mathbf{S_e} + g_h \mu \mathbf{B} \cdot \mathbf{S_h} + J(\mathbf{S_e} \cdot \mathbf{S_h})$$

where μ is the Bohr magneton, g_e and g_h the g-values for the excited-state electron and a deep hole state, respectively, and J is the exchange interaction between them. The spin-Hamiltonian can be solved in terms of eigenfunctions of total spin, $|S, M\rangle$, given by

$$\Phi_1 = |1,1\rangle$$
$$\Phi_2 = [(1-Q)|0,0\rangle + (1+Q)|1,0\rangle]/[2(1+Q^2)]^{-\frac{1}{2}}$$
$$\Phi_3 = [-(1+Q)|0,0\rangle + (1-Q)|1,0\rangle]/[2(1+Q^2)]^{-\frac{1}{2}}$$
$$\Phi_4 = |1,-1\rangle$$

where

$$Q = J/\left\{ (g_e - g_h)\mu B + [(g_e - g_h)^2 \mu^2 B^2 + J^2]^{\frac{1}{2}} \right\}$$

and eigenvalues given by

$$E_1 = (g_e + g_h)\mu B/2 + J/4$$
$$E_2 = [(g_e - g_h)^2 \mu^2 B^2 + J^2]^{\frac{1}{2}}/2 - J/4$$
$$E_3 = -[(g_e - g_h)^2 \mu^2 B^2 + J^2]^{\frac{1}{2}}/2 - J/4$$
$$E_4 = -(g_e + g_h)\mu B/2 + J/4.$$

To calculate the change in electron capture rate to the centre on resonance it can be assumed that pair creation probabilities for each of the M spin states are basically equal to 1/M at room temperature, and the pair dissociated probabilities per unit time per pair for each spin state are equal and basically given by the emission rate of the excited-state electron

14

$$P_d = (\sigma_n \upsilon_{th} N_C / M) \exp(-\Delta E / kT)$$

where ΔE is energy depth of the excited state of the defect centre. The dissociation rate should be of order 10^{10} s^{-1} with $\Delta E / kT \approx 0$ at room temperature for $\sigma_n \approx 10^{16}$ cm^2 the estimated value for neutral recombination centre at Si/SiO$_2$ interfaces. As expected, the dissociation rate, P_d, decreases as $\Delta E / kT$ increases.

The rate of final capture and recombination of the excited-state electron depends on the excited-state eignstate. The usual rigid spin selection rule can not be applied here as the non-radiative transitions have only a limited spin memory. However, the singlet to singlet transition rate is still expected to be significantly greater than the triplet to singlet rate so the probabilities, per unit time, for the readjustment stage of recombination for the pure triplet state, P_t, compared to the pure singlet state, P_s, gives $P_s \gg P_t$. The shortest possible time for P_s is given by the Heisenberg uncertainty principle from the observed EDMR linewidth of approximately 1 mT to be of order 10^8s^{-1}. The readjustment probabilities for each of the allowed spin state energies are linear combinations of P_s and P_t. For a given state the probability must be greater than or equal to P_t and less than or equal to P_s. For example for the weak exchange case considered above the probabilities, P_k, are given by:

$$P_1 = P_t$$
$$P_2 = P_s/2 + P_t/2$$
$$P_3 = P_s/2 + P_t/2$$
$$P_4 = P_s.$$

From these, by solving the steady state rate equation occupancy numbers for the spin states can be determined and hence steady-state spin-dependent carrier capture rates determined. A general expression for the change in the capture rate on spin resonance can be obtained. For the specific case considered it can be shown that the change in recombination rate, U, on resonance is given by

$$\Delta U / U \approx \Delta P_s P_{kj} / (2P_d)^2 \approx 10^{-4}$$

with P_s and P_{kj} of order 10^8s^{-1} and $P_d \approx 10^{10}$s^{-1}. The magnitude of the change is consistent with the experiment. The approach is shown to limit the magnitude of the effect predicted by KSM. To date, due to the lack of experimental studies the implications and validity of the approach have yet to be fully tested.

EDMR Spectrometer Design

The primary focus of this investigation was the construction of a electrically-detected magnetic resonance spectrometer. A schematic of the basic features of the spectrometer system is given in Figure 1. The device under test is placed in the microwave resonant structure. The present award allowed an EDMR unit to be constructed and installed on a B_{max} = 2.1 T Bruker

BE-30 EPR magnet funded by EPSRC joint research equipment grant GR/L26377. This consists of magnetic field modulation coils and amplifier compatible with the magnet and microwave

Figure 1 - Simple Schematic of EDMR Spectrometer
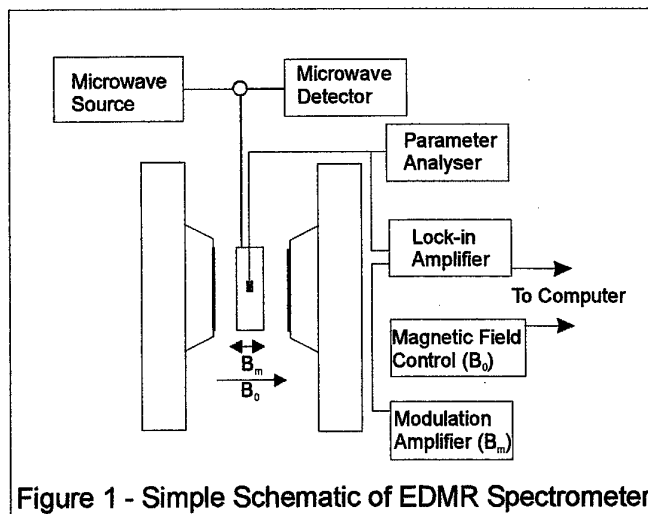
resonant structure, a EG&G 5209 lock-in amplifier, a Kiethley source-measure unit and specially constructed low-noise dc device driving circuits.

The construction strategy was altered through the period of the award as a result of our being awarded an EPRSC grant: *"Defect characterisation of materials for large-area electronics using electron paramagnetic resonance"* (GR/L89754) which enabled us to install a Bruker EMX electron paramagnetic resonance spectrometer system in the laboratory. The complex and difficult tasks of microwave bridge construction were delayed and design philosophy altered to plan for an integrated multifrequency EPR/EDMR facility utilising the modular design of the Bruker spectrometer, see Figure 2. Integration to the Bruker system is not complete at this stage but we are able to control both the Bruker and the EDMR unit externally and so have a fully operational 9 GHz EDMR spectrometer.

Figure 2 - Schematic of Electron Magnetic Resonance Facility
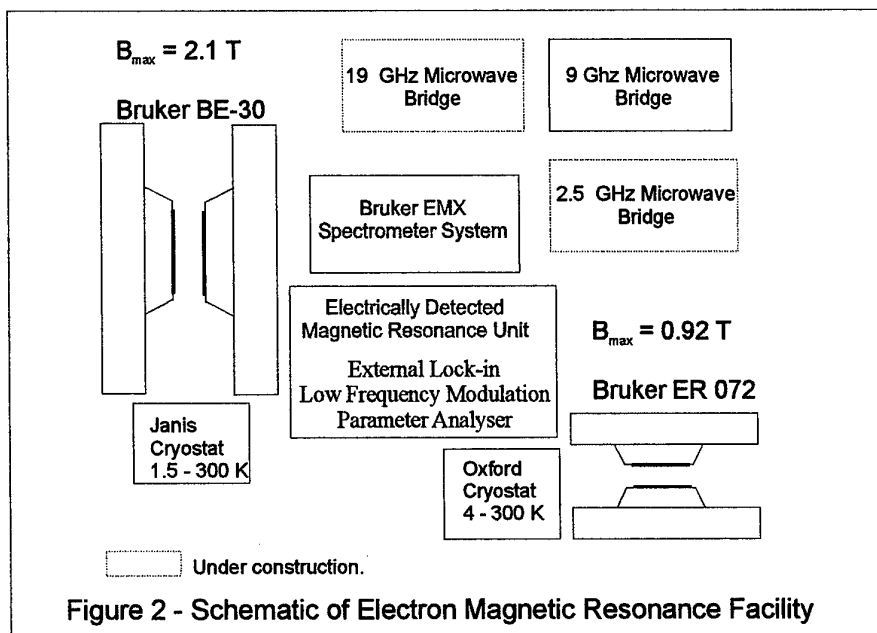
Calibration of the spectrometer system for magnetic field modulation frequencies from 40 to 100 kHz was completed. Necessary control software was written and initially testing of the EDMR system was successfully completed using several 1N4007 silicon junction diodes.

EDMR Results

For test purposes the initial device studied was a commercial 1N4007 n^+p silicon diode. A spectrum is shown in Figure 3. This shows a metal ion impurity, as inferred from the position (g-value) of the resonance. It is confidently predicted that modifications to the spectrometer, which are now in hand, will result in a dramatic improvement in the signal-to-noise ratio. The dependence of EDMR signal amplitude on forward bias current was measured and found to be consistent with previous work, see Figure 4. [18] A series of magnetic field modulation frequencies from 40 Hz to 400 Hz were also investigated for several values of forward bias current, see Figures 5 and 6.

17
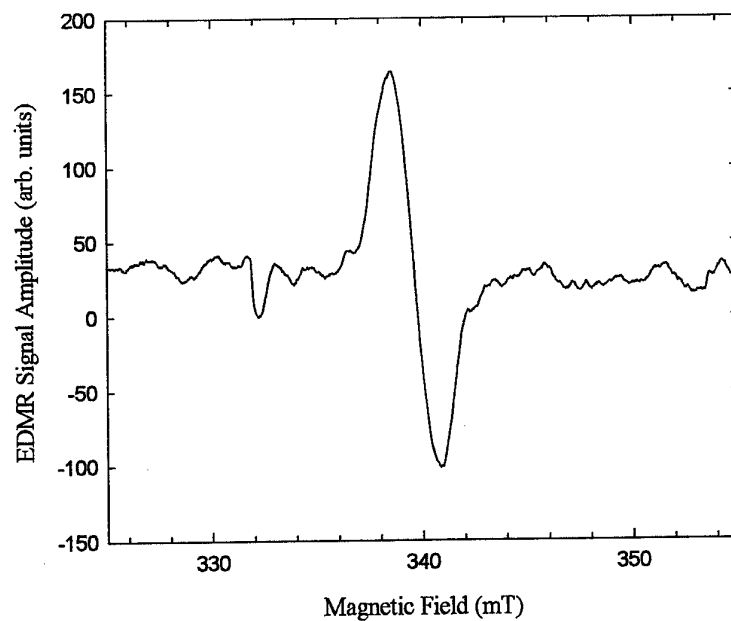
Figure 3 – 1N4007 junction diode EDMR spectrum
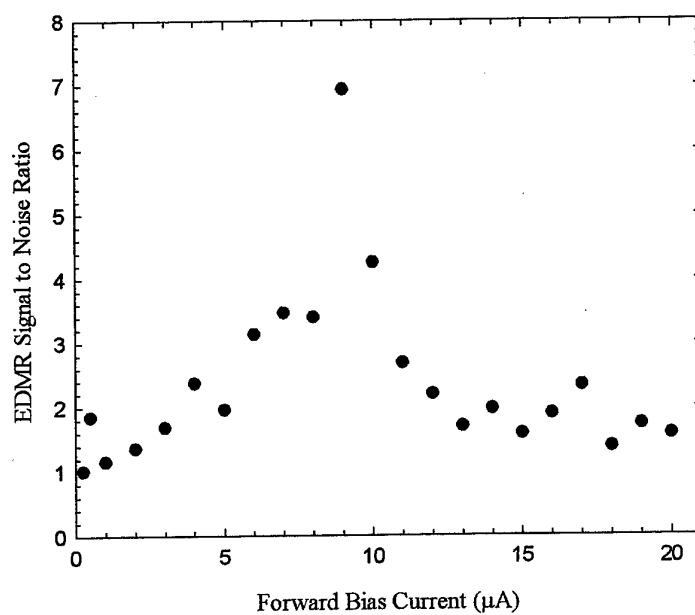
Figure 4 – 1N4007 EDMR signal to noise against forward bias current.
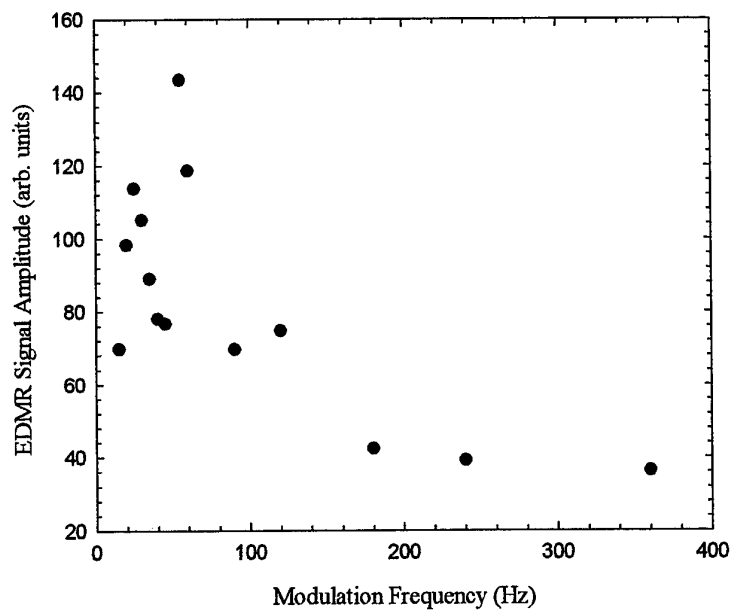
Figure 5 – 1N4007 EDMR signal against modulation frequency for I = 10 μA.
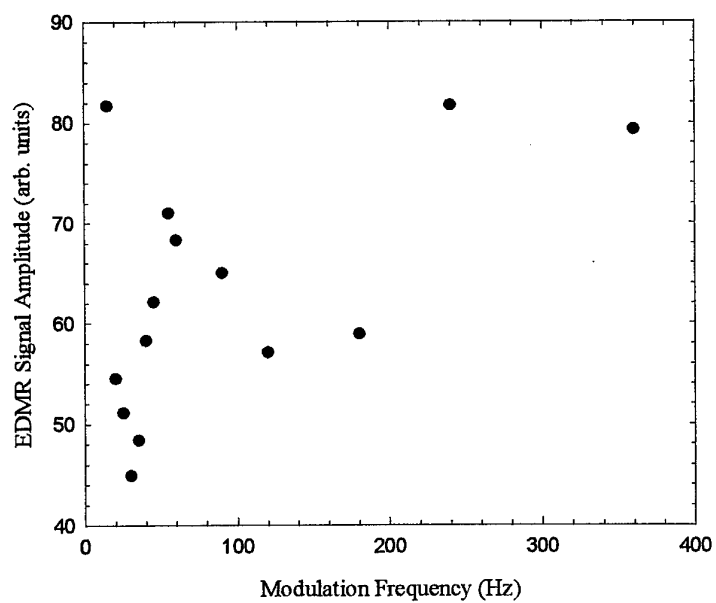
Figure 6 – 1N4007 EDMR signal against modulation frequency for I = 9 μA.

Electron Magnetic Resonance of Platinum in Silicon

In this section the literature is reviewed on EDMR measurements on silicon junction diodes and on platinum containing paramagnetic defects in silicon. The reported spin-Hamiltonian parameters for platinum related defect centres in silicon are then used to simulate the EPR spectra for the applied magnetic field, B_0, rotated in the (111) plane. Spectra for B_0 parallel to [111] are also simulated. These correspond to the common experimental situations for EDMR studies of 1N400X diodes were the device is rotated about its long axis or the field is applied along the axis. Simulations were performed using EPRNMR which solves the appropriate spin-Hamiltonian by "exact" diagonalisation. [24] The microwave frequency 9.5 GHz was used for all simulated spectra.

The first EDMR experiment on a commercial silicon p-n junction diode (1N4005) was carried out by Solomon. [18] The resonance was a single line with a g-value of 2.005(3). A study of a gate controlled silicon n^+p diode reported a single resonance with a similar g-value, 2.0063(5). [25] The first EDMR experiments to provide evidence that signals from metallic ions could be detected were performed by Rong et al. [3] Isotropic resonances were found for 1N4007 and 1N4005 diodes with g-values 1.965 and 1.984. A more detailed room temperature study of 1N4007 diodes from International Rectifier Inc detected a spectrum with partially resolved hyperfine structure. [1] The field was varied in the (111) plane and it was found the g-value varied from 1.999(2) to 2.012(2). The intensity of the two partially resolved lines was found to be consistent with 33.8% abundant I = ½ ^{195}Pt. The splitting gave an approximate value for the hyperfine coupling constant of 280(80) MHz. From a comparison of the calculated (111) g-maps shown above and the observed g-value variation it is concluded that the EDMR Pt-related centre is not fully consistent with those known from EPR, however, the discrepancy may lead to further important insights in to the EDMR mechanism.

Christmann et al studied silicon p-n diode BY448 and were able to study EDMR with the applied field parallel to the (111) plane and perpendicular to the plane along <111>. [26] The signal was shown to have $g_{||}$ = 1.97(1) and $g_\perp$ = 2.04(1) with respect to the (111) plane. Stich et al reported EDMR measurements on 1N4007 diodes manufactured Fagor, at room temperature a single isotropic resonance at g = 2.006(2) was observed. [2] At temperatures below 100 K a complex, anisotropic, EDMR spectrum was then observed which was tentatively assigned to the P_i-C_s defect. Xiong and Miller have also studied silicon junction diodes. [27] They observed an anisotropic resonance from 1N4007 GP875 diodes and reported g-values of $g_{||}$ = 2.002(1) and $g_\perp$ = 2.007(1) for the magnetic field parallel to a <111> direction and within the (111) plane, respectively. It was proposed the resonance was due to silicon divacancies.

A recent study of 1N400x type silicon diodes found one group of devices that showed multiple signals. [28] Three dominant signals were found to have g-ellipsoid that is rotationally symmetric about the diode axis, presumed to be a <111>. They were all found to have a $g_{||}$ ≈ 1.967 within the (111) plane but had $g_\perp$ with values of 2.028, 2.046 and 2.072 normal to the plane, parallel to <111>. The spectrum with $g_\perp$ = 2.046 has been observed by other workers. Comparison of these values with the reported spin-Hamiltonians for platinum related centres, described in this section, confirm they are not consistent. Also recently Kamigaki et al have measured specially fabricated silicon $p^+ - n^- - n^+$ junction diodes. [4] Platinum was diffused

20

through the junction region at different temperatures allowing two diodes with Pt concentrations differing by approximately a factor two to be studied. A spectrum showing two features was obtained and shown to be due to two defect centres. The g-values for the signals for B_0 in the (111) plane were given as 1.991 and 1.978, these values are close to the value given by Christmann *et al* of 1.97(1). [26]

Platinum is used as a dopant in silicon to achieve fast carrier recombination. It is known to be a common dopant in 1N400x type silicon diodes. From studies in bulk crystalline silicon it is known to commonly incorporate by substitution on a silicon site, Pt_s. This centre results in three levels in the band gap: Pt_s (–/0) at E_c – 0.243 eV, Pt_s (0/+) at E_v + 0.330 eV, and Pt_s (+/++) at E_v + 0.067 eV.[29-33] The EPR spectrum attributed to the negative charge state, Pt_s^-, was identified by Ludwig & Woodbury.[34,35] The orthorhombic C_{2v} symmetry was assumed to be due to a <100> distortion of the platinum taking it off centre toward one of the two pairs of silicon atoms. Later this simple interpretation was challenged by Henning & Egelmeers who reported results of strain-modulated EPR experiments on the spectrum in which a lower C_{1h} symmetry was assumed on the basis of the symmetry of the stain coupling tensor. The observed substructure on the spectrum was interpreted as due to a further interaction with an interstitial Pt^0 nearest neighbour. [36] However, experiments on isotopically enriched platinum showed this model to be incorrect.[37] The identification of the Pt_s (–/0) at E_c – 0.243 eV was made firm by comparison of photo-EPR and junction space-charge methods.[38] More recently an EPR study at two microwave frequencies and using strain, both perpendicular and parallel to the magnetic field direction, has been made.[39] The spin-Hamiltonian parameters are shown in Table I. The measured strain tensor was found to have C_{2v} symmetry and the Pt and Si hyperfine and superhyperfine structure were consistent with an isolated substitutional Pt. Two models have been shown to be consistent with the observed spin-Hamiltonian, one in which the platinum in a dihedral configuration bound predominantly to two Si neighbours, the other the Pt is put into a silicon vacancy and the orthorhombic symmetry results from a Jahn Teller distortion. [40,41]

Table I - EPR Parameters for Pt_{Si} from Anderson et al. [39]

Centre	symmetry	S	axis	g	A_{Pt}
Pt_{Si}	orthorhombic	½	$z \parallel \langle 100 \rangle$	2.0789	380.7 MHz
			$y \parallel \langle 110 \rangle$	1.4265	557.6 MHz
			$x \parallel \langle 110 \rangle$	1.3865	443.7 MHz

Using the principal values shown in Table I the variation in g for the centre in the (111) plane was calculated and is shown in Figure 7. The resulting EPR spectra for two orientations of B_0 in the (111) are shown in Figure 8. The spectrum for B_0 parallel to <111> is shown in Figure 11.

In addition to isolated substitutional Pt, platinum pairs and even a six-platinum cluster have been reported. [42-44] The spin-Hamiltonian parameters for these Pt complex centres are given in Table II. The Pt-Pt complex first reported by von Bardeleben was further studied by Hone and a second pair spectrum identified. [42,44] The original centre, Pt-Pt type I, has been simulated and the g-map for the (111) plane is shown in Figure 9. That for the type II centre is shown in Figure 10.
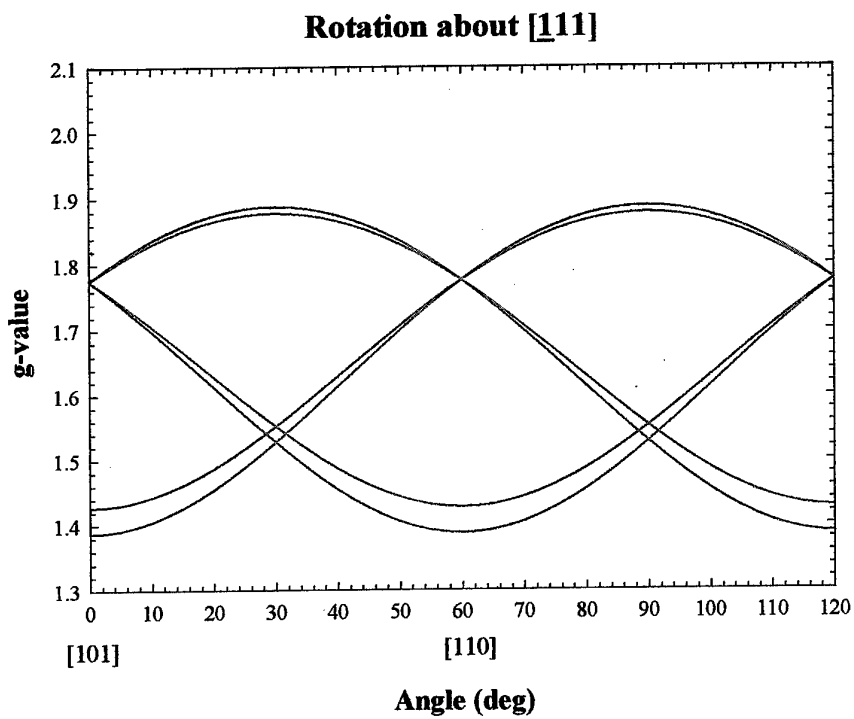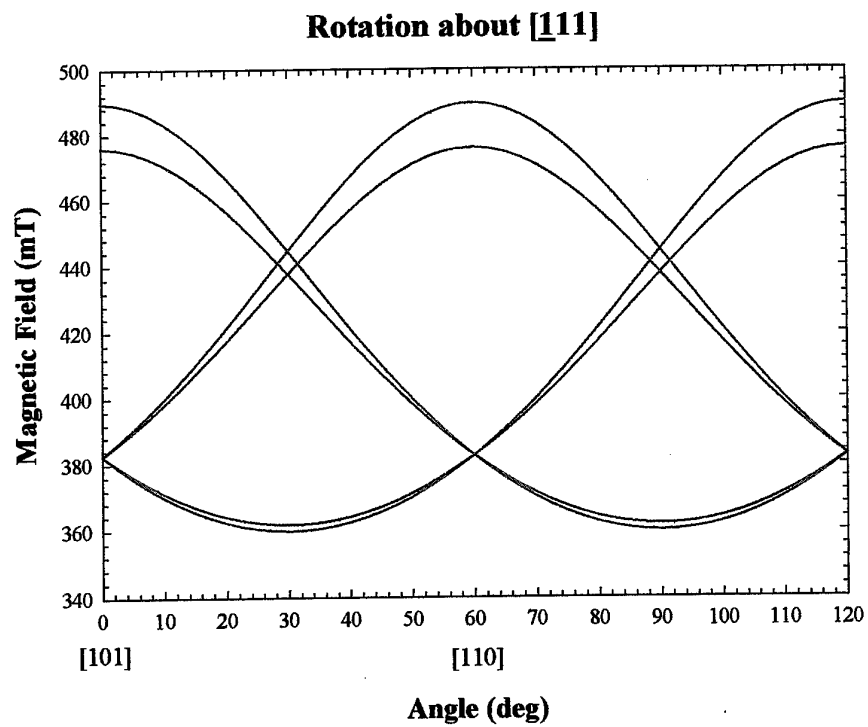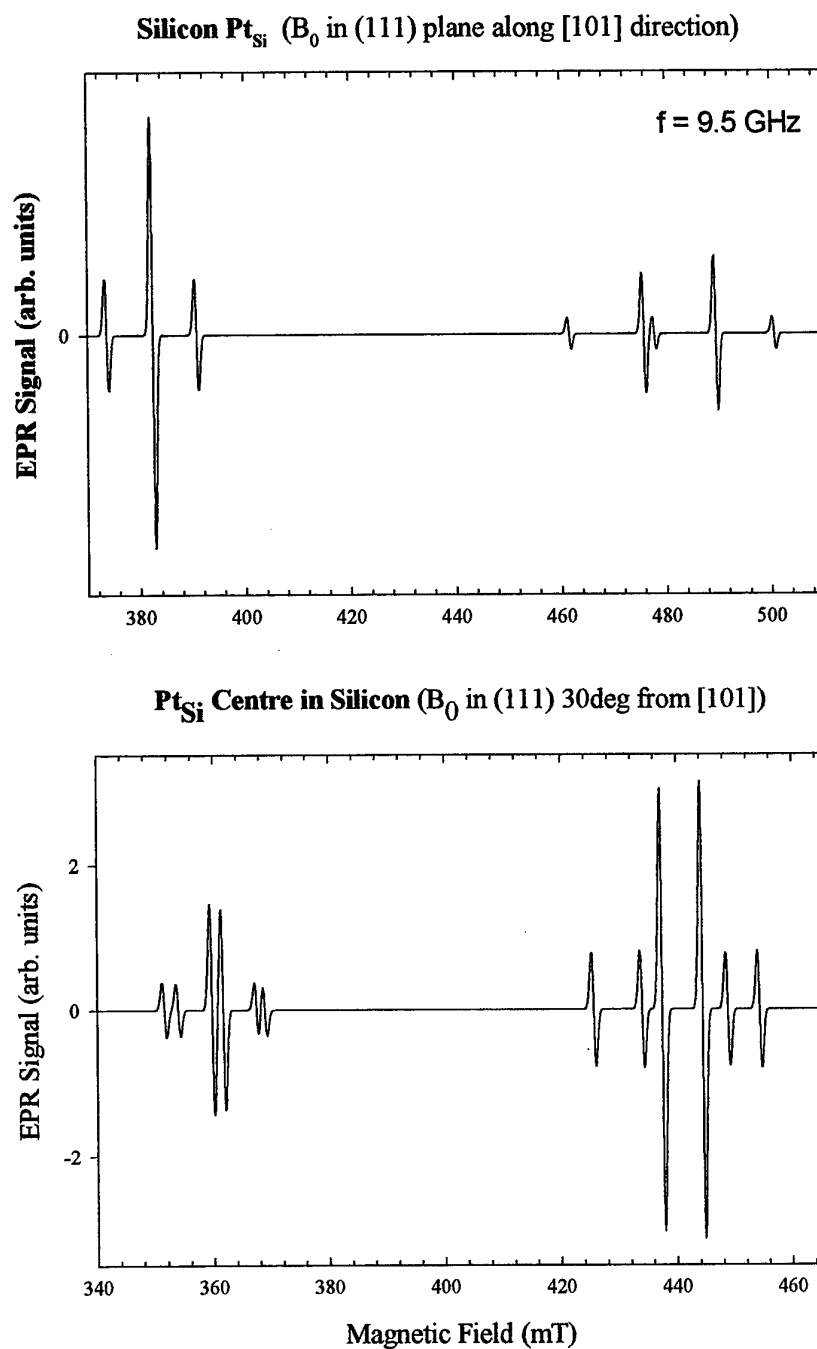
Rotation about [$\bar{1}$11]

Rotation about [$\bar{1}$11]

Figure 7 – Pt$_{Si}$ g-map

Silicon Pt$_{Si}$ (B$_0$ in (111) plane along [101] direction)

Pt$_{Si}$ Centre in Silicon (B$_0$ in (111) 30deg from [101])

Figure 8 – Pt$_{Si}$ EPR Spectra for two field orientations in (111)

Rotation about [111]

Rotation about [111]

Figure 9 – Pt-Pt type I *g*-map

Rotation about [$\underline{1}$11]

Rotation about [$\underline{1}$11]
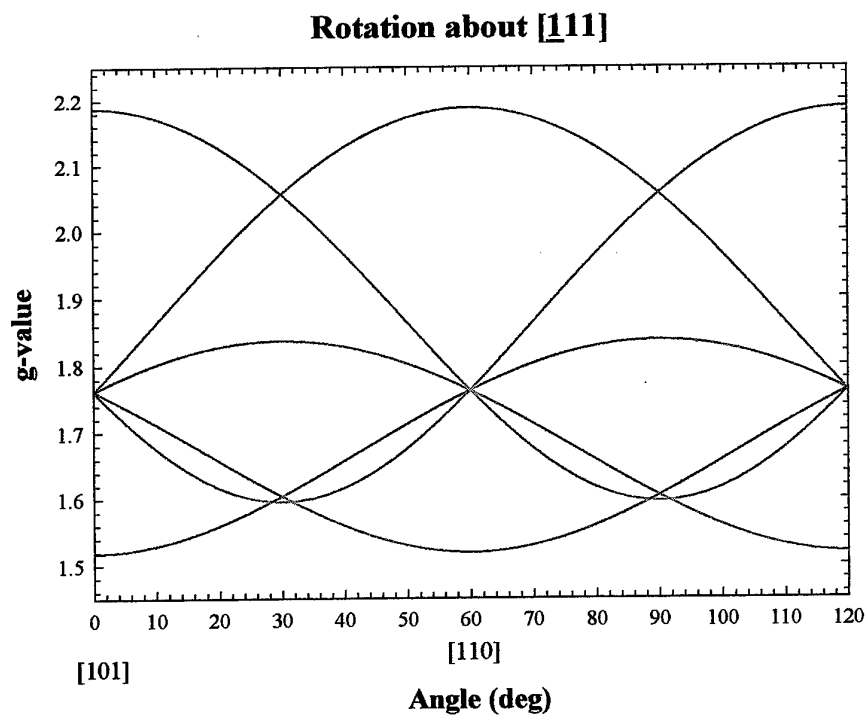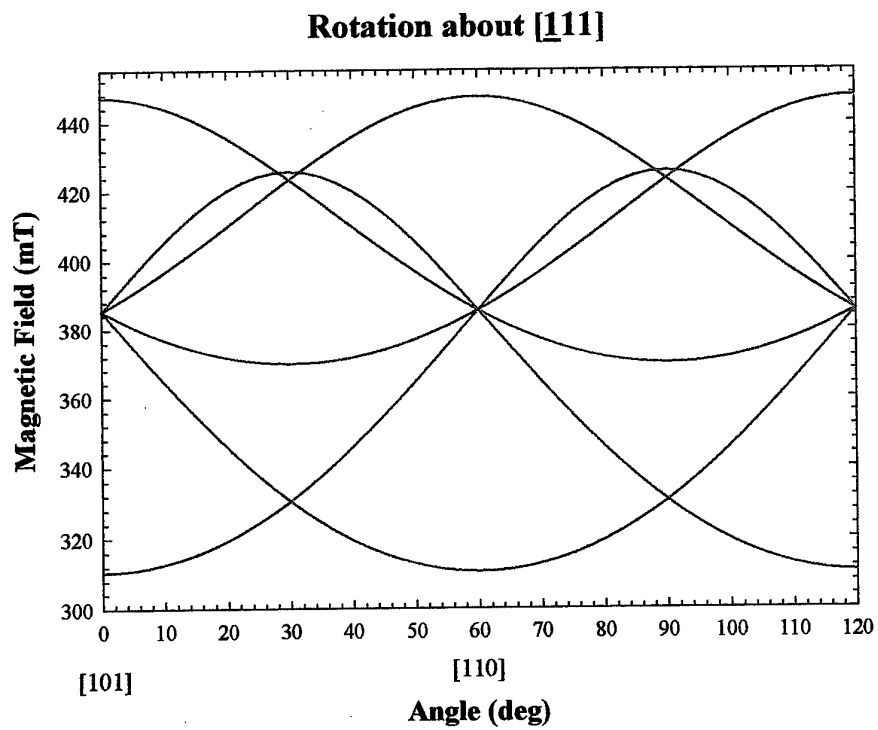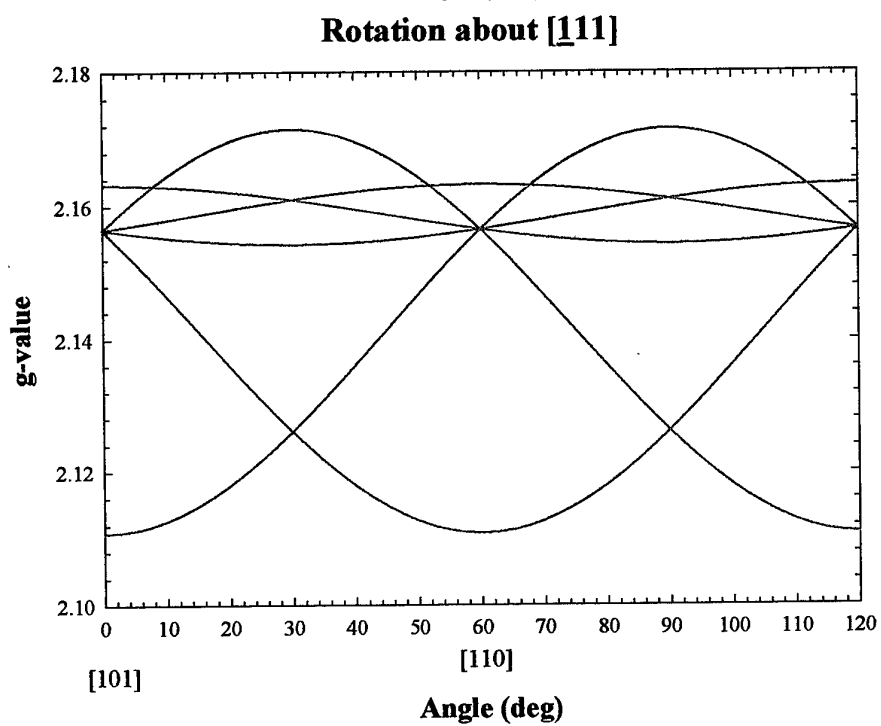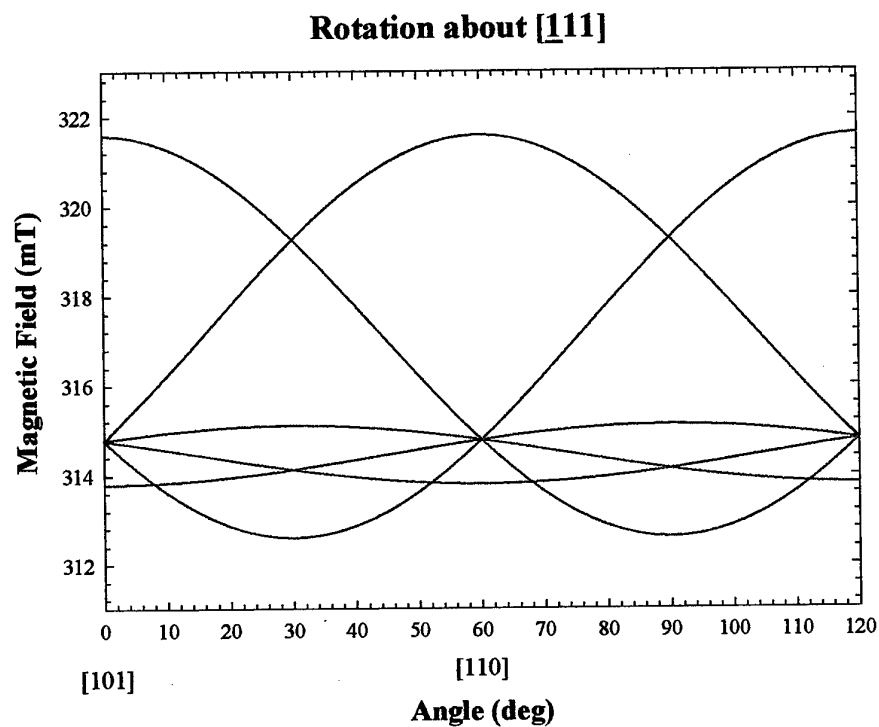
Figure 10 – Pt-Pt type II *g*-map
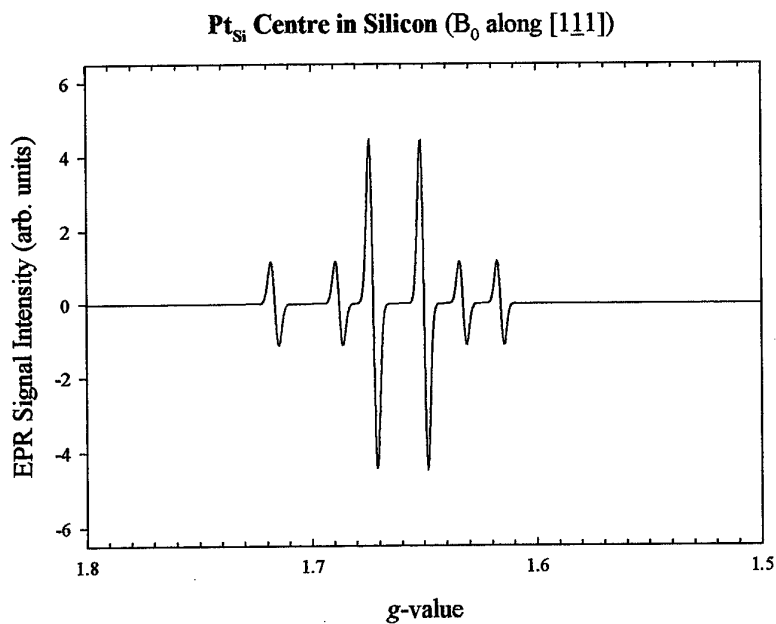
Figure 11 – Pt$_{Si}$ EPR Spectrum B$_0$ along $\left[1\bar{1}1\right]$

Table II - EPR Parameters for Pt cluster defects

Centre	symmetry	S	axis	g	A$_{Pt}$
Pt-Pt	orthorhombic	½	z $\parallel$ $[001]$	1.6317	207 MHz $\parallel$ $\left[1\bar{1}1\right]$
	Von Bardeleben (Ref [42])		y $\parallel$ $\left[\bar{1}10\right]$	2.1869	156 MHz $\parallel$ $[110]$
			x $\parallel$ $[110]$	1.5181	256 MHz $\parallel$ $\left[\bar{1}12\right]$
Pt-Pt type II	orthorhombic Höhne (Ref [44])	½	z $\parallel$ $[001]$	2.1755	†
			y $\parallel$ $\left[\bar{1}10\right]$	2.1107	
			x $\parallel$ $[110]$	2.1631	
6-Pt	trigonal	½	z $\parallel$ $\langle 111\rangle$	$g_{\parallel} = 1.917$	‡
	Höhne & Juda (Ref [43])			$g_{\perp} = 2.117$	

† Hyperfine tensor information complex, see Höhne. [44]

‡ Hyperfine tensor information complex, see Höhne & Juda. [43]

Two EPR spectra attributed to platinum-oxygen centre has also been reported, see Table III. [45] The spectra are monoclinic and were observed from all n- and p-type Czochralski (Cz) and float zone (FZ) silicon studied, the concentration approaching that of the isolated platinum centre for annealed Cz silicon. The presence of oxygen at the centre was inferred from the observation that the concentration was consistently higher in the Cz compared to FZ silicon. The (111) g-maps for the two oxygen centres Or-1Pt(A) and Or-1Pt(B) are shown in Figures 12 and 13, respectively. It should also be noted that in the original work of Woodbury and Ludwig a second spectrum was observed at higher temperatures. [34] This was very tentatively assigned to a Pt oxygen pair defect. The spin-Hamiltonian parameters are shown in Table IV.

Table III - EPR parameters for O containing Pt centres in Silicon from Juda et al. [45]

Centre	symmetry	S	axis	g	A_{Pt}
Or-1Pt(A)	monoclinic	$\frac{1}{2}$	$z=Z=\zeta \| \langle 110 \rangle$ [a]	1.1653	36.0 MHz
			$y \| \langle 110 \rangle$, $Y \angle 50° y$	1.2455	95.9 MHz
			$x \| \langle 001 \rangle$, $X \angle 50° x$	2.6226	95.9 MHz
Or-1Pt(B)	monoclinic	$\frac{1}{2}$	$z=Z=\zeta \| \langle 110 \rangle$ [a]	1.7072	
			$y \| \langle 110 \rangle$, $Y \angle 58° y$	1.8804	
			$x \| \langle 001 \rangle$, $X \angle 58° x$	2.4196	

[a] Defined as parallel to the x-axis for Pt_{Si} from Anderson et al. [39]

Table IV - EPR Parameters for Pt(II) Woodbury and Ludwig

Centre	symmetry	S	axis	g	A_{Pt}
Pt(II)	trigonal	½	$z \| \langle 111 \rangle$	$g_{\|} = 2.021$	467.7 MHz
				$g_{\perp} = 2.126$	185.9 MHz

The Pt(II) centre is an example of a spin-Hamilitonian with axial symmetry about the <111> type direction. The g-map for the (111) plane has been simulated and is shown in Figure 14. The spectra for two orientations in the (111) plane are given in Figure 15 and that for the field parallel to a <111> direction in Figure 16.

Rotation about [1̲11]
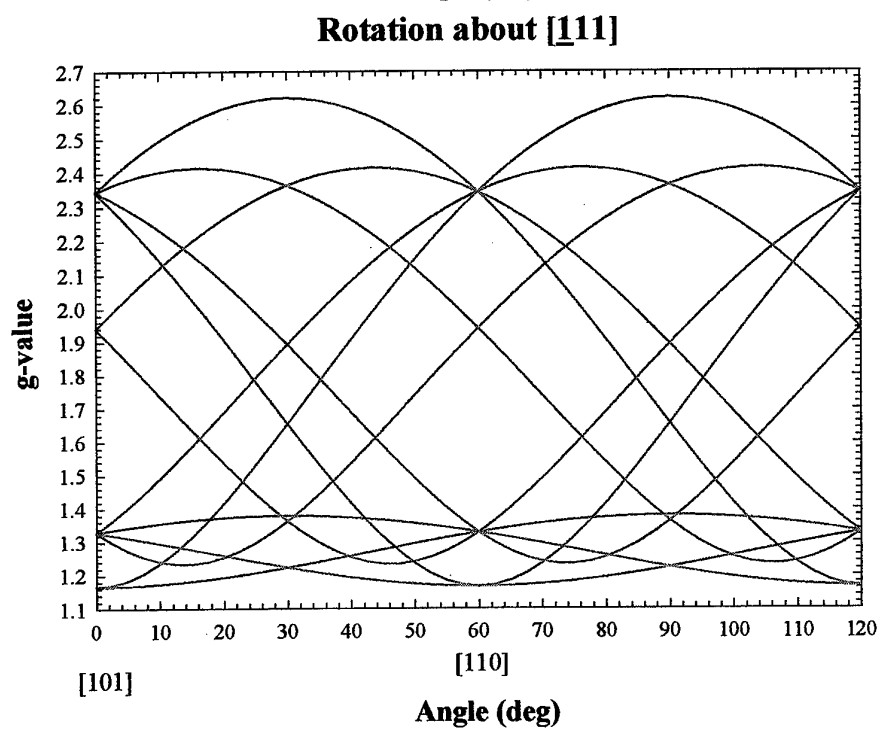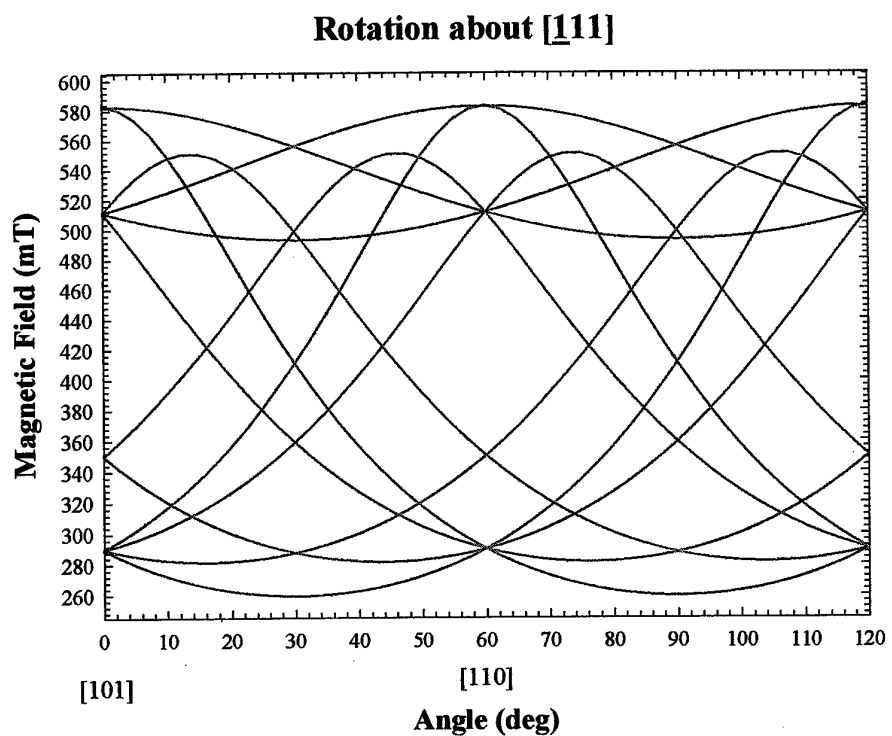

Magnetic Field (mT) vs **Angle (deg)**

[101]   [110]

Rotation about [1̲11]

g-value vs **Angle (deg)**

[101]   [110]

Figure 12 – Oxygen Platinum Centre Or-1Pt(A) *g*-map

Rotation about [1̄11]

Rotation about [1̄11]
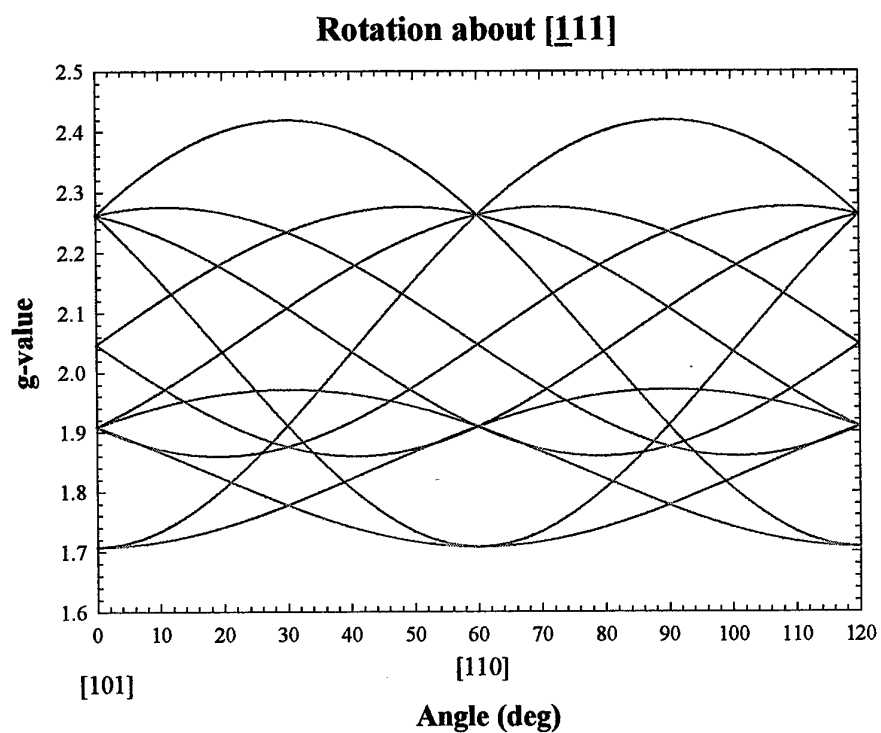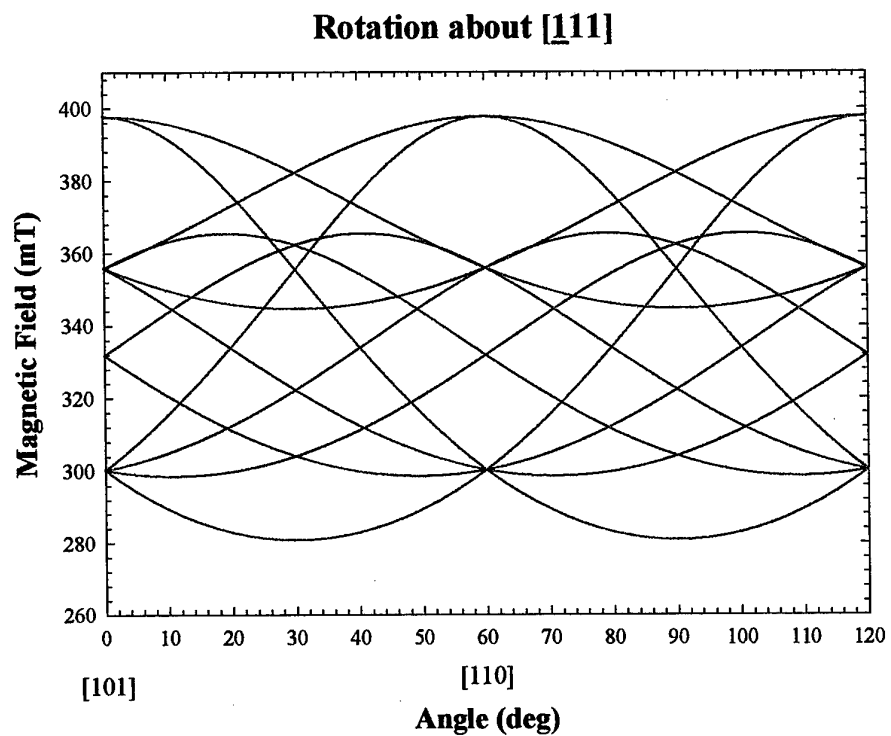
Figure 13 – Oxygen Platinum Centre Or-1Pt(B) *g*-map

Rotation about [$\underline{1}$11]

[101]

[110]

Angle (deg)

Rotation about [$\underline{1}$11]

[101]

[110]

Angle (deg)

Figure 14 – Pt(II) *g*-map

Pt(II) Centre in Silicon (B_0 in ($\underline{1}$11) along [101])

Pt(II) Centre in Silicon (B_0 in ($\underline{1}$11) 30deg from [101])
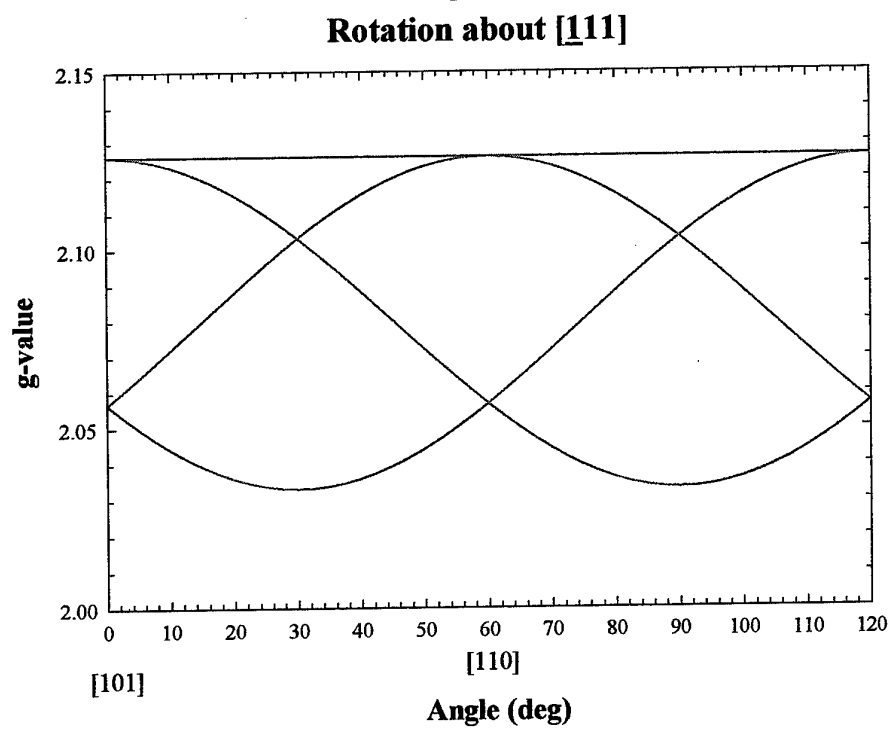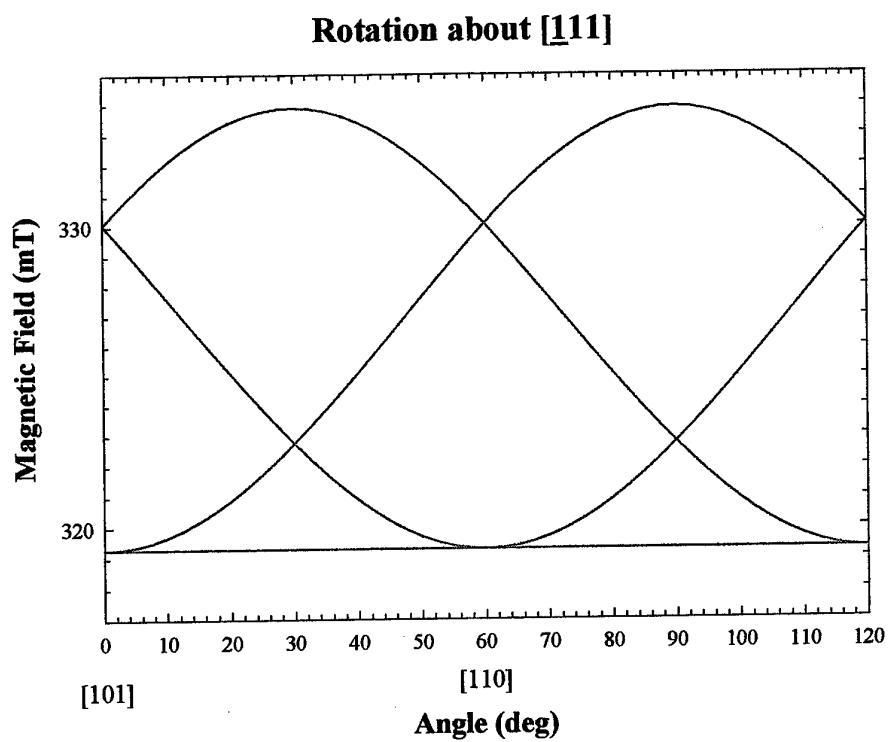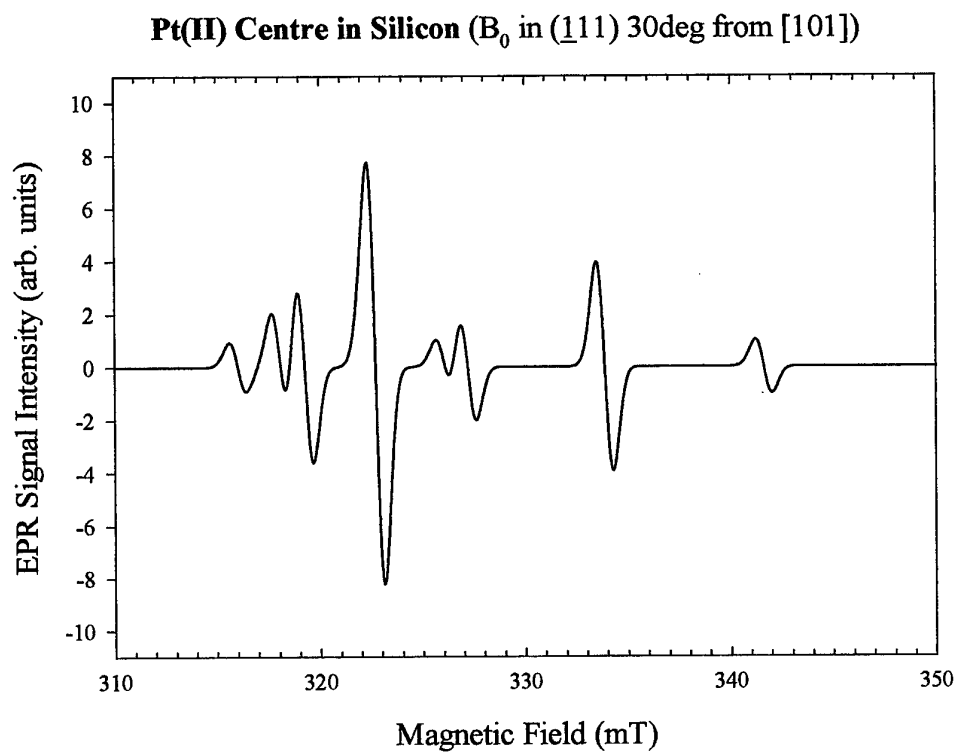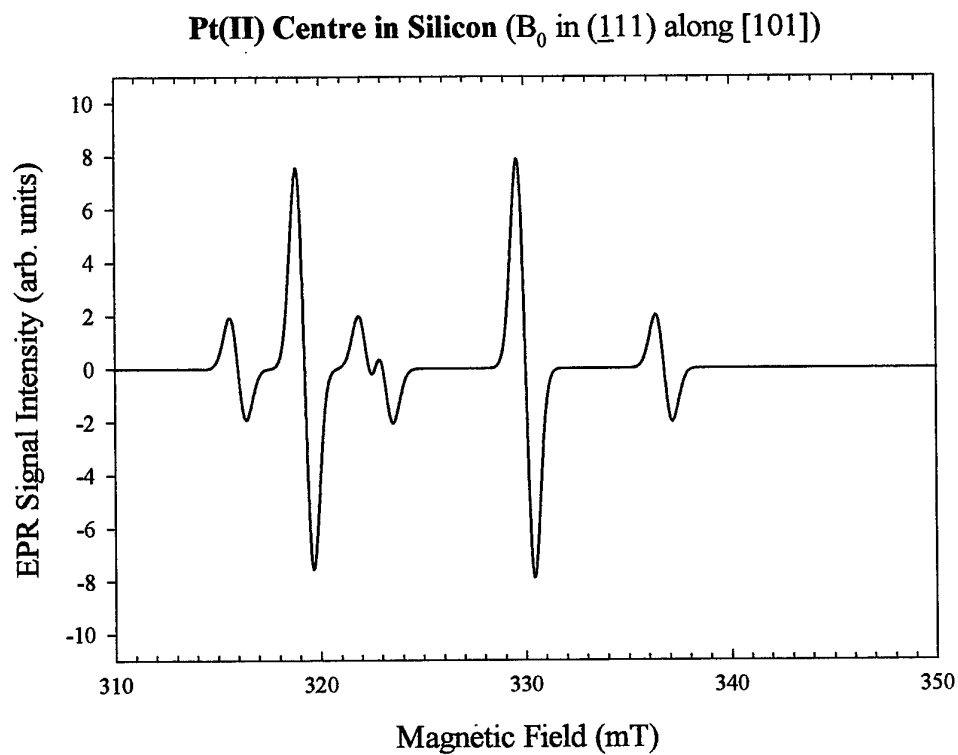
Figure 15 – Pt(II) EPR Spectra for two field orientations in (111)

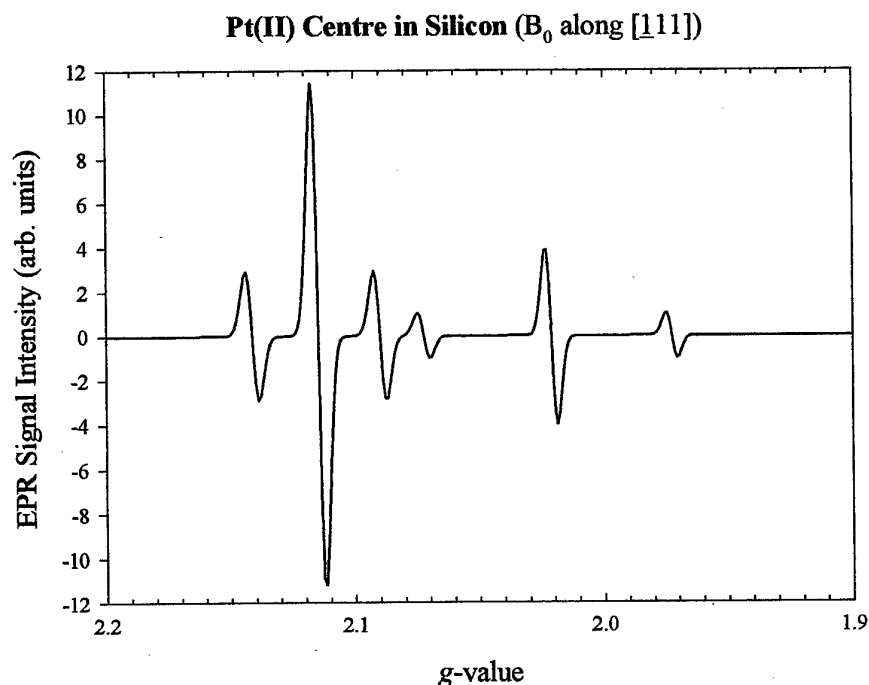## Pt(II) Centre in Silicon (B_0 along [$\bar{1}$11])

Figure 16 – Pt(II) EPR Spectrum B_0 along $\left|\bar{1}11\right|$

Platinum related EPR spectra have also been studied for silicon in which hydrogen has been incorporated. It has been reported that hydrogen can passivate the electrical activity of the deep centre introduced by platinum incorporation. [46,47] Two EPR spectra have been reported for platinum-hydrogen complexes, one attributed to Pt-H_2 the second labelled Si-NL53. [48,49] The Pt-H_2 centre was further studied by Uftring et al using infrared spectroscopy and EPR.[50] Small corrections to the spin-Hamiltonian parameters were reported and a complete study of the hydrogen superhyperfine structure made, see Table V. This allowed a more accurate model to be proposed. Electrical characterisation of hydrogen related Pt centres has assigned a level at E_c – 0.50 eV to Pt-H, two levels at E_c – 0.18 eV and E_v – 0.40 eV to Pt-H_2, and a level at E_v – 0.30 eV to Pt-H_3. [51,52] The level positions for Pt-H_2 are in reasonable agreement with those obtained from theory and in approximate agreement with those derived from IR and EPR measurements. [50,53]

The (111) g-map for the Pt-H_2 centre described by Uftring et al is shown in Figure 17. The associated EPR spectra for B_0 along [101] and 30° from this direction are shown in Figure 18 and that for B_0 along [111] in Figure 19.

Table V - EPR parameters for H containing Pt centres in Silicon

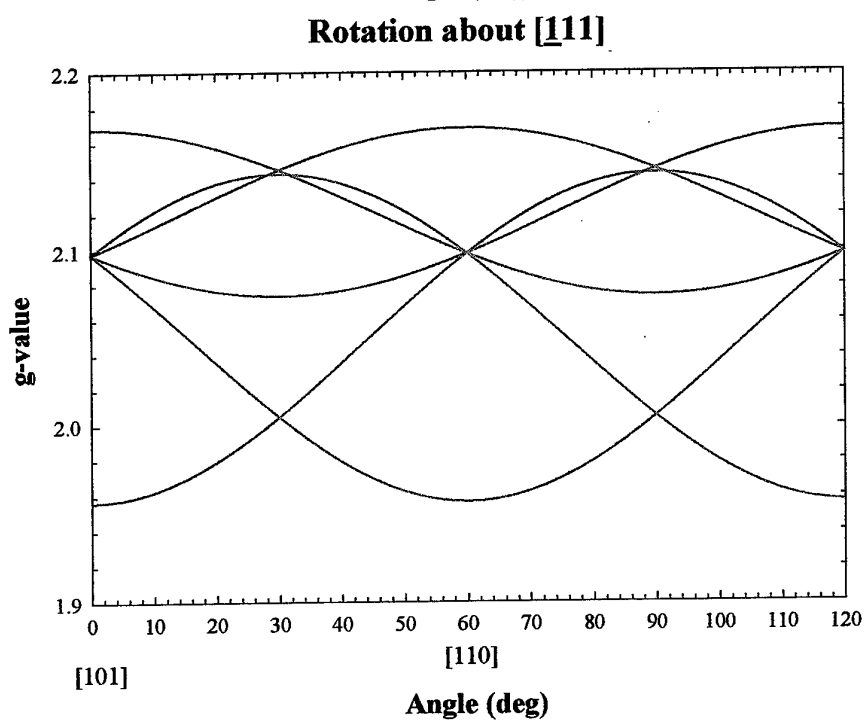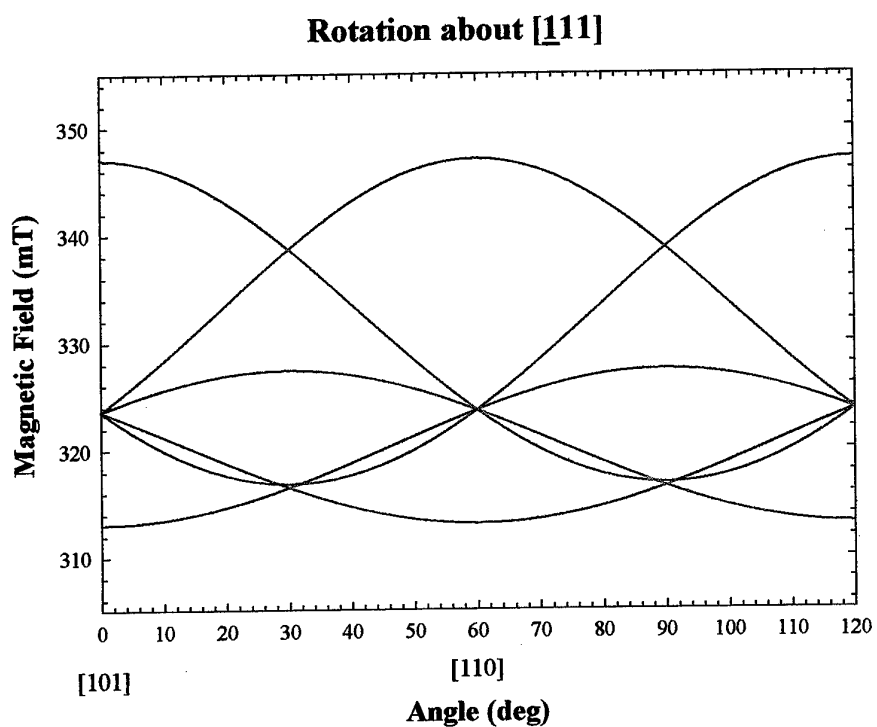| Centre	symmetry	S	axis	g	A_{Pt}
Pt-H$_2$	orthorhombic	$\frac{1}{2}$	$\parallel [100]$	2.1299	172 MHz
	after Uftring *et al.* (Ref.[50])		$\parallel [011]$	2.1683	238 MHz
			$\parallel [0\bar{1}1]$	1.9563	542 MHz
	orthorhombic	$\frac{1}{2}$	$\parallel [100]$	2.1299	175.7 MHz
	after Höhne *et al.*(Ref.[49])		$\parallel [011]$	2.1683	237.3 MHz
			$\parallel [0\bar{1}1]$	1.9563	541.2 MHz
Si-NL53	trigonal	$\frac{1}{2}$		$g_{\parallel} = 2.5082$	349.4 MHz
				$g_{\perp} = 2.0206$	327.3 MHz $\parallel [1\bar{1}0]$
					432.7 MHz 12.4° to $[11\bar{1}]$ in $(1\bar{1}0)$

Rotation about [1̲11]

Rotation about [1̲11]

Figure 17 – Pt-H₂ Centre g-map

Pt$_{Si}$-H$_2$ Centre in Silicon (B$_0$ in ($\underline{1}$11) along [101]) no H-hyperfine
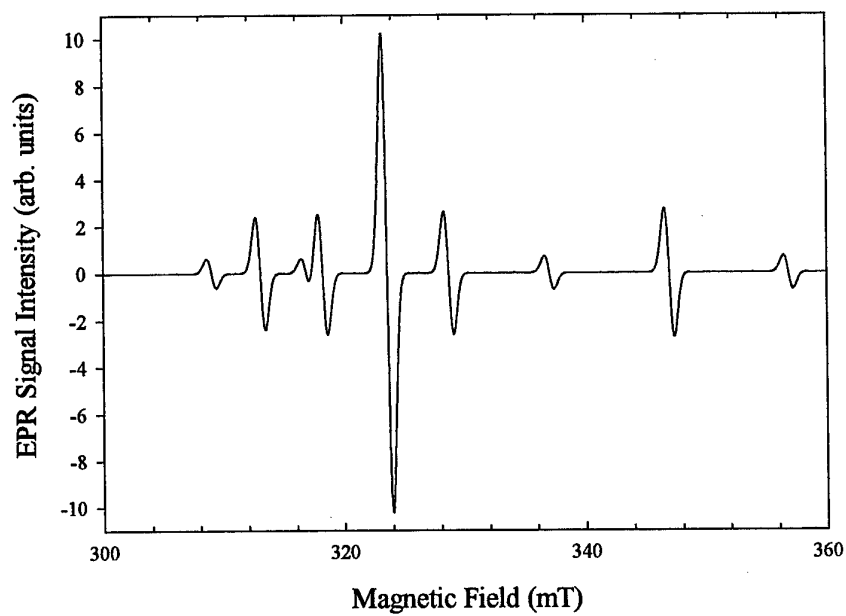
Pt$_{Si}$-H$_2$ Centre in Silicon (B$_0$ in ($\underline{1}$11) 30deg from [101]) no H-hyperfine
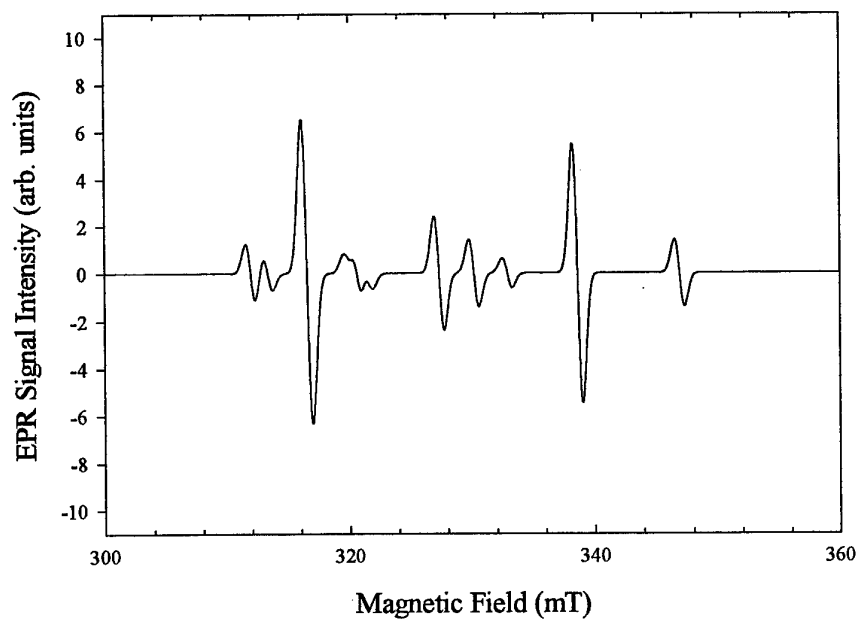
Figure 18 – Pt-H$_2$ EPR Spectra for two field orientations in (111)

Pt-H₂ Centre in Silicon (B₀ along [1$\underline{1}$1])
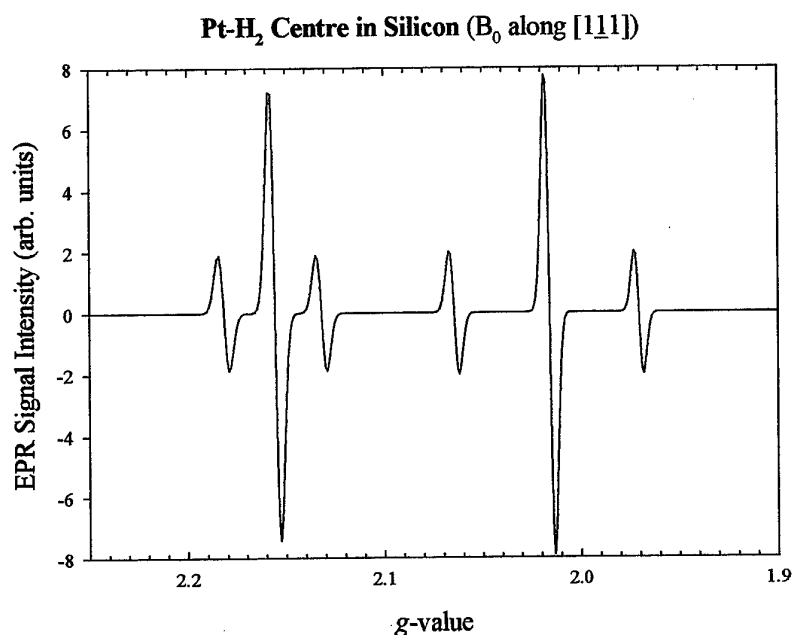
Figure 19 - Pt-H₂ EPR Spectrum B₀ along $\left[1\,\overline{1}\,1\right]$

Silicon crystals co-doped with both Pt and carbon were found to exhibit two EPR spectra, one associated with one Pt atom (cr-1Pt), the other with three Pt atoms (cr-3Pt). The number of carbon atoms involved could not be determined. [54] Both centres were found to have electronic spin S = 3/2 and a large crystal field splitting giving the characteristic $g_{eff,\parallel} \approx 2$ and $g_{eff,\perp} \approx 2 g_{eff,\parallel}$, see Table VI. The centres were distinguished by the observed hyperfine structure and small differences in g-values.

Table VI - EPR parameters for carbon containing Pt centres in Silicon from Scheerer et al. [54]

Centre	symmetry	S	axis	g	A$_{Pt}$
cr-1Pt	trigonal	$\frac{3}{2}$	z || $\langle 111 \rangle$	$g_{eff,\parallel}$ = 2.1111	36.0 MHz
				$g_{eff,\perp}$ = 4.0770	45.0 MHz
cr-3Pt	trigonal	$\frac{3}{2}$	z || $\langle 111 \rangle$	$g_{eff,\parallel}$ = 2.0358	15.0 MHz
				$g_{eff,\perp}$ = 4.0770	37.5 MHz

In addition to complexes with hydrogen, oxygen or carbon, complexes with lithium have also been reported, see Table VII.

Table VII - EPR parameters for Li containing Pt centres in Silicon from Alteheld et al. [55]

Centre	symmetry	S	axis	g	A_{Pt}
Pt-Li	orthorhombic	$\frac{1}{2}$	$z \parallel [001]$	1.769	134 MHz
			$y \parallel [\bar{1}10]$	1.746	247 MHz
			$x \parallel [\bar{1}10]$	2.250	118 MHz
Pt-Li$_3$	trigonal	$\frac{1}{2}$	$z \parallel \langle 111 \rangle$	$g_{\parallel} = 1.898$	696 MHz
				$g_{\perp} = 2.165$	321 MHz

The simple Pt-Li centre was also simulated. The (111) *g*-map is shown in Figure 21 and the EPR spectra for two field orientations in the plane are given in Figure 22. The spectrum for B₀ along [111] is given in Figure 20.
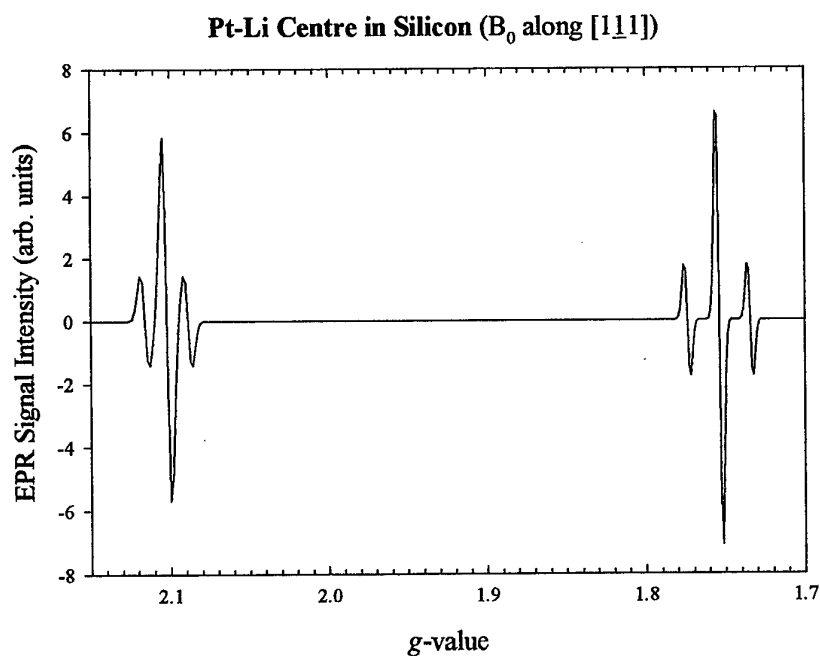

Pt-Li Centre in Silicon (B$_0$ along [1$\underline{1}$1])

Figure 20 - Pt-Li EPR Spectrum B$_0$ along $[1\bar{1}1]$

37

Rotation about [1̲11]

Rotation about [1̲11]
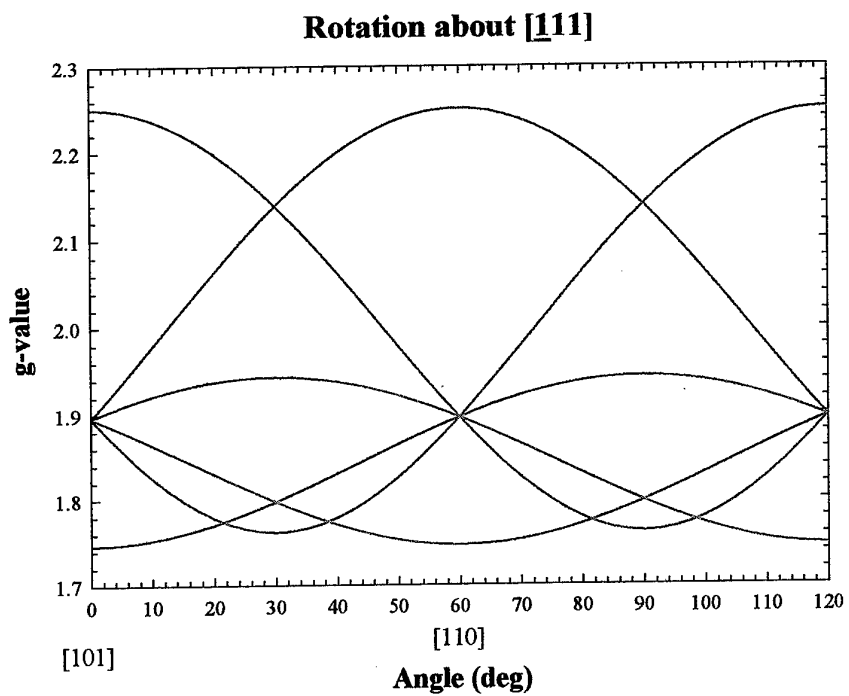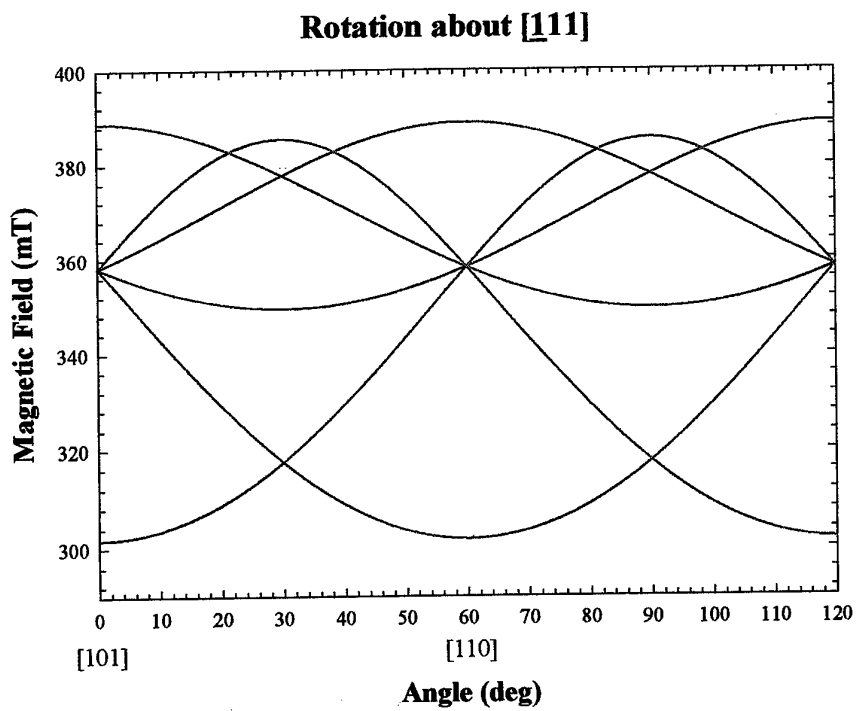
Figure 21 – Pt-Li Centre *g*-map

Pt-Li Centre in Silicon (B_0 in ($\underline{1}$11) along [101])

Pt-Li Centre in Silicon (B_0 in ($\underline{1}$11) 30deg from [101])

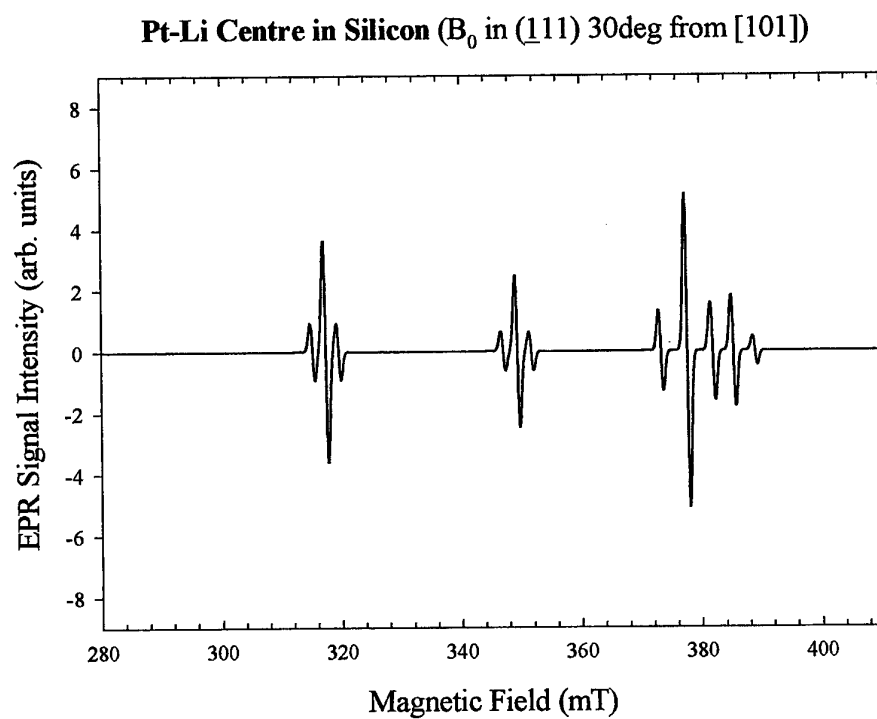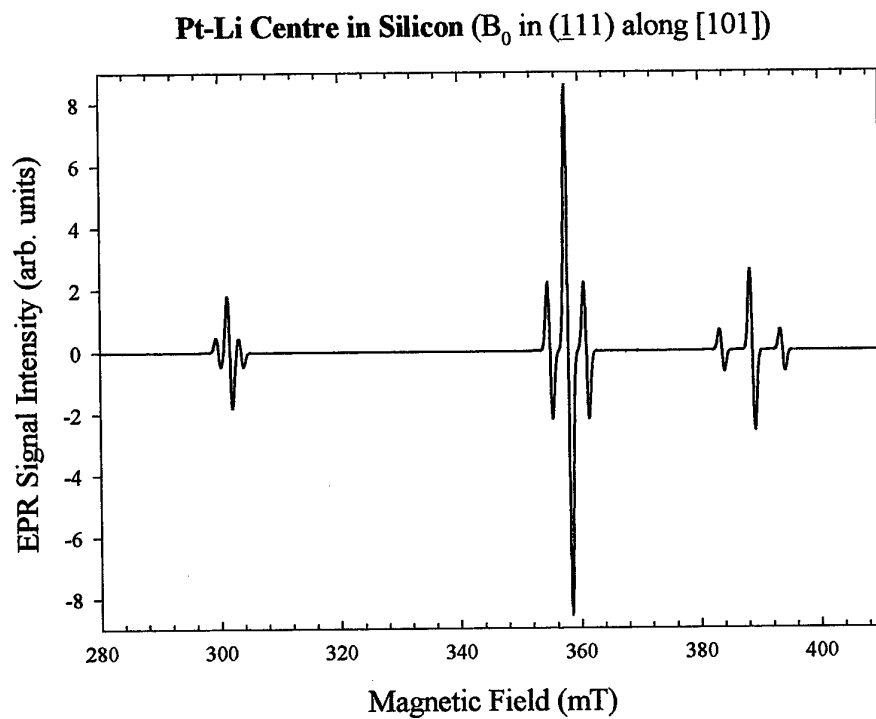**Figure 22 – Pt-Li EPR Spectra for two field orientations in (111)**

Comparison of the known platinum related defect centres in silicon to the spin-Hamiltonian parameters reported from EDMR experiments on silicon junction diodes shows that, to-date no direct correspondence exists. However, the match is close and, as mentioned previously, the discrepancy may lead to further insights in to the mechanism involved.

Concluding Remarks

In summary this award has allowed an EDMR unit to be successfully installed, necessary control software to be written, and the complete 9 GHz system tested. Preliminary results from 1N4007 silicon junction diodes have been recorded as a function of forward bias current and using magnetic field modulation frequencies in the range 40 to 5 kHz.

In addition the literature on paramagnetic platinum related defect centres in silicon has been reviewed. The reported spin-Hamiltonian parameters were then used to simulate EPR spectra for rotation in the (111) plane and for the applied magnetic field along <111> type directions. These simulations were used to compare to EDMR results from silicon junction diodes were it has been proposed that the signals detected are due to platinum containing defects. No exact correlation could be found between the g-values of the simulated spectra and those reported from silicon junction diode EDMR spectra. The deviation of these g-values is an important area for further work.

Further Work

Samples silicon diode structures have been received from Professor S.A. Lyon, Princeton University, where preliminary room temperature data has been taken. This work will be extended at Dundee to include temperature dependence down to 3.8 K and a more complete study of the angular dependence of the observed resonances. The aim is to obtain a full description of the spin-Hamiltonian and to gain further insight into the mechanism of EDMR. The small g-value discrepancies highlighted above will be investigated.

Further, the exciting possibility that the technique will give key insights into spin processes in semiconductors of direct relevance to the implementation of quantum computing devices will also be explored.

Literature cited

1. Rong, F. C., Gerardi, G. J., Buchwald, W. R., Poindexter, E. H., Umlor, M. T., Keeble, D. J. & Warren, W. L. Electrically Detected Magnetic-Resonance of a Transition-Metal Related Recombination Center in Si P-N Diodes. *Applied Physics Letters* **60**, 610-612 (1992).

2. Stich, B., Gruelichweber, S., Spaeth, J. M. & Overhof, H. Electrically Detected Electron-Paramagnetic-Resonance Of a Deep Recombination Center In a Silicon Diode. *Semiconductor Science and Technology* **8**, 1385-1392 (1993).

3. Rong, F., Poindexter, E. H., Harmatz, M. & Buchwald, W. R. Electrically detected magnetic resonance in p-n junction diodes. *Solid State Commun.* **76**, 1083-6 (1990).

4. Kamigaki, Y., Miyazaki, T., Yoshihiro, N., Watanabe, K. & Yokogawa, K. Two signals in electrically detected magnetic resonance of platinum- doped silicon p-n junctions. *Journal of Applied Physics* **84**, 2193-2198 (1998).

5. Graeff, C. F. O., Brandt, M. S., Stutzmann, M. & Powell, M. J. Defect Creation In Amorphous-Silicon Thin-Film Transistors. *Physical Review B-Condensed Matter* **52**, 4680-4683 (1995).

6. Kawachi, G., Graeff, C. F. O., Brandt, M. S. & Stutzmann, M. Carrier Transport In Amorphous Silicon-Based Thin-Film Transistors Studied By Spin-Dependent Transport. *Physical Review B-Condensed Matter* **54**, 7957-7964 (1996).

7. Keeble, D. J. DAAH04-95-1-0375 (Army Research Office, 1995).

8. Rong, F. C., Buchwald, W. R., Poindexter, E. H., Warren, W. L. & Keeble, D. J. Spin-Dependent Shockley-Read Recombination of Electrons and Holes In Indirect-Band-Gap Semiconductor p-n-Junction Diodes. *Solid-State Electronics* **34**, 835-841 (1991).

9. Honig, A. Neutral-impurity scattering and impurity zeeman spectroscopy in semiconductors using highly spin-polarized carriers. *Physical Review Letters* **17**, 186-8 (1966).

10. Maxwell, R. & Honig, A. Neutral-impurity scattering in silicon with highly spin-polarized electrons. *Phys. Rev. Lett.* **17**, 188-90 (1966).

11. Lepine, D. J. & Prejean, J. J. in *Proceedings of the 10th International Conference on the Physics of Semiconductors* (eds. Keller, S. P., Hencal, J. C. & Stern, F.) 805-8 (Us Atomic Energy Commission, Washington, Dc, 1970).

12. Lepine, D. J. Spin-dependent recombination on silicon surface. *Phys. Rev. B* **6**, 436-41 (1972).

13. Solomon, I. in *Amorphous Semiconductors* (eds. Brodsky, M. H., LeComber, P. & Spear, W.) (Springer-Verlag, 1979).

14. Abragam, A. *Principles of Nuclear Magnetism* (Oxford University Press, 1961).

15. Ruzyho, J., Shiota, I., Miyamota, N. & Nishizawa, J. *J. Electrochem. Soc.* **123**, 26 (1976).

16. Wosinski, T. & Figielski, T. Spin-dependent recombination at dislocations in silicon. *Physica Status Solidi B* **71**, K73-76 (1975).

17. Lepine, D., Grazhulis, V. A. & Kaplan, D. in *13th International Conference on the Physics of Semiconductors* (ed. Fumi, F. G.) 1081-4 (Tipografia Marves, 1976).

18. Solomon, I. Spin-dependent recombination in a silicon p-n junction. *Solid State Communications* **20**, 215-17 (1976).

19.   Solomon, I., Biegelsen, D. & Knights, J. C. Spin-dependent photoconductivity in n-type and p-type amorphous silicon. *Solid State Communications* **22**, 505-8 (1977).

20.   L'vov, V. S., Tretyak, O. V. & Kolomiets, I. A. Spin-dependent carrier recombination on a silicon surface. *Soviet Physics Semiconductors* **11**, 661-4 (1977).

21.   White, R. M. & Gouyet, J. F. Theory of spin-dependent effects in silicon. *Physical Review B* **16**, 3596-602 (1977).

22.   Kaplan, D., Solomon, I. & Mott, N. F. Explanation of the large spin - dependent recombination effect in semiconductors. *Journal of Physics (Paris) Letters* **39**, L51-4 (1978).

23.   Shockley, W. & Read, W. T. Statistics of the recombination of holes and electrons. *Physical Review* **87**, 835-42 (1952).

24.   Computer Program EPR-NMR *(Department of Chemistry, University of Saskatchewan, Canada)* (1993).

25.   Kaplan, D. & Pepper, M. Spin dependent surface recombination in silicon p-n junctions: the effect of irradiation. *Solid State Communications* **34**, 803-805 (1980).

26.   Christmann, P., Wetzel, C., Meyer, B. K., Asenov, A. & Endros, A. Spin Dependent Recombination in Pt-Doped Silicon P-N-Junctions. *Applied Physics Letters* **60**, 1857-1859 (1992).

27.   Xiong, Z. & Miller, D. J. Identification of the Common Electrically Detected Magnetic-Resonance Signal From a Si Diode. *Journal of Applied Physics* **78**, 4895-4898 (1995).

28.   Hornmark, E. T., Lyon, S. A. & Poindexter, E. H. Electrically-Detected Magnetic Resonance in Silicon Junction Diodes. *Bulletin of the American Physical Society* **44**, 1047 (1999).

29.   Lemke, H. The Possible Existence of Repulsive Centers With Large Capture Sections in Silicon. *Physica Status Solidi a-Applied Research* **86**, K39-K43 (1984).

30.   Zimmermann, H. & Ryssel, H. Trivalent Character of Platinum in Silicon. *Applied Physics Letters* **58**, 499-501 (1991).

31.   Miller, M. D. *Journal of Applied Physics* **47**, 2569 (1976).

32.   Evwaraye, A. O. & Sun, E. *Journal of Applied Physics* **47**, 3172 (1976).

33.   Braun, S. & Grimmeiss, H. G. *Journal of Applied Physics* **48**, 3883 (1977).

34.   Woodbury, H. H. & Ludwig, G. W. *Phys. Rev.* **126**, 466 (1962).

35.   Ludwig, G. W. & Woodbury, H. H. in *Solid State Physics: Advances in Research and Applications* (eds. Seitz, F. & Turnbull, D.) 223 (Academic Press, New York, 1962).

36.   Henning, J. C. M. & Egelmeers, E. C. J. Strain-Modulated Electron-Spin-Resonance Study of Pt- in Silicon. *Physical Review B-Condensed Matter* **27**, 4002-4012 (1983).

37.   Milligan, R. F., Anderson, F. G. & Watkins, G. D. Electron-Paramagnetic Resonance of Pt- in Silicon - Isolated Substitutional Pt Versus Pt-Pt Pairs. *Physical Review B-Condensed Matter* **29**, 2819-2820 (1984).

38.   Omling, P., Emanuelsson, P. & Grimmeiss, H. G. Photoelectron Paramagnetic-Resonance of Pt- in Silicon. *Physical Review B-Condensed Matter* **36**, 6202-6205 (1987).

39.   Anderson, F. G., Milligan, R. F. & Watkins, G. D. Epr Investigation of Pt- in Silicon. *Physical Review B-Condensed Matter* **45**, 3279-3286 (1992).

40.   Ammerlaan, C. A. J. & Vanoosten, A. B. Electronic-Structure of Platinum in Silicon. *Physica Scripta* **T25**, 342-347 (1989).

41.   Anderson, F. G., Ham, F. S. & Watkins, G. D. Vacancy-Model Interpretation of Epr-Spectrum of Si-Pt. *Physical Review B-Condensed Matter* **45**, 3287-3303 (1992).

42. Vonbardeleben, H. J., Stievenard, D., Brousseau, M. & Barrau, J. Electron-Paramagnetic-Res Observation of a Platinum Pair Complex in Si. *Physical Review B-Condensed Matter* **38**, 6308-6311 (1988).

43. Hohne, M. & Juda, U. Complexing in Silicon Induced By Surface-Reactions - Electron-Paramagnetic Resonance Detection of a 6-Platinum Cluster. *Journal of Applied Physics* **72**, 3095-3101 (1992).

44. Hohne, M. Electron-Paramagnetic Resonance of a Platinum Pair Complex in Silicon. *Physical Review B-Condensed Matter* **45**, 5883-5886 (1992).

45. Juda, U., Scheerer, O., Hohne, M., Riemann, H., Schilling, H. J., Donecker, J. & Gerhardt, A. Oxygen-related 1-platinum defects in silicon: An electron paramagnetic resonance study. *Journal of Applied Physics* **80**, 3435-3444 (1996).

46. Pearton, S. J. & Haller, E. E. Palladium-Related and Platinum-Related Levels in Silicon - Effect of a Hydrogen Plasma. *Journal of Applied Physics* **54**, 3613-3615 (1983).

47. Pearton, S. J., Corbett, J. W. & Stavola, M. *Hydrogen in Crystalline Semiconductors* (Springer-Verlag, Berlin, 1992).

48. Williams, P. M., Watkins, G. D., Uftring, S. & Stavola, M. Structure-Sensitive Spectroscopy of Transition-Metal-Hydrogen Complexes in Silicon. *Physical Review Letters* **70**, 3816-3819 (1993).

49. Hohne, M., Juda, U., Martynov, Y. V., Gregorkiewicz, T., Ammerlaan, C. A. J. & Vlasenko, L. S. Epr Spectroscopy of Platinum-Hydrogen Complexes in Silicon. *Physical Review B-Condensed Matter* **49**, 13423-13429 (1994).

50. Uftring, S. J., Stavola, M., Williams, P. M. & Watkins, G. D. Microscopic Structure and Multiple Charge States of a Pth2 Complex in Si. *Physical Review B-Condensed Matter* **51**, 9612-9621 (1995).

51. Sachse, J. U., Sveinbjornsson, E. O., Jost, W., Weber, J. & Lemke, H. Electrical properties of platinum-hydrogen complexes in silicon. *Physical Review B-Condensed Matter* **55**, 16176-16185 (1997).

52. Sachse, J. U., Weber, J. & Sveinbjornsson, E. O. Hydrogen-atom number in platinum-hydrogen complexes in silicon. *Physical Review B-Condensed Matter* **60**, 1474-1476 (1999).

53. Jones, R., Resende, A., Oberg, S. & Briddon, P. R. The electronic properties of transition metal hydrogen complexes in silicon. *Materials Science and Engineering B-Solid State Materials For Advanced Technology* **58**, 113-117 (1999).

54. Scheerer, O., Hohne, M., Juda, U. & Riemann, H. Carbon-related platinum defects in silicon: An electron paramagnetic resonance study of high spin states. *Journal of Applied Physics* **82**, 3456-3461 (1997).

55. Alteheld, P., Greulichweber, S., Spaeth, J. M., Weihrich, H., Overhof, H. & Hohne, M. Aggregate Defects of Gold and Platinum With Lithium in Silicon .1. Magnetic-Resonance Investigations. *Physical Review B-Condensed Matter* **52**, 4998-5006 (1995).